New particle formation at a peri-urban agricultural site

Julien Kammer, Leila Simon, Raluca Ciuraru, Jean-Eudes Petit, Florence Lafouge, Pauline Buysse, Sandy Bsaibes, Ben Henderson, Simona M Cristescu, Brigitte Durand, et al.

New Particle Formation at a peri-urban agricultural site

Authors

Julien Kammer[1,2,3,*], Leila Simon[1], Raluca Ciuraru[2], Jean-Eudes Petit[1], Florence Lafouge[2], Pauline Buysse[2], Sandy Bsaibes[1,2], Ben Henderson[4], Simona M. Cristescu[4], Brigitte Durand[2], Oliver Fanucci[2], Francois Truong[1], Valerie Gros[1] and Benjamin Loubet[2]

Affiliations

[1]Laboratoire des Sciences du Climat et de l'Environnement, CEA-CNRS-UVSQ, IPSL, Université Paris-Saclay, 91191 Gif-sur-Yvette, France

[2]INRA, UMR ECOSYS, INRA, AgroParisTech, Université Paris-Saclay, 78850 Thiverval-Grignon, France

[3] Aix Marseille Univ, CNRS, LCE, Marseille, France

[4]Department of Analytical Chemistry and Chemometrics, IMM, Radboud University, Nijmegen, the Netherlands

[*]Corresponding author :

Julien Kammer

UMR 7376 Laboratoire de Chimie de l'Environnement (LCE)

Université d'Aix-Marseille

3 place Victor Hugo - Case 29

CS 80249 - 13331 Marseille CEDEX 3 - France

Mail : julien.kammer@univ-amu.fr

Highlights

- NPF has been observed at a mixed peri-urban agricultural site
- NPF occurred during both the daytime and the night-time
- Night-time NPF events are suggested to be related to agricultural emissions, whereas daytime events are not

Abstract

New Particle Formation (NPF) is a major source of ultrafine particles that affect both air quality and climate. Despite emissions from agricultural activities having a strong potential to lead to NPF, little is known about NPF within agricultural environments. The aim of the present study was to investigate the occurrence of NPF events at an agricultural site, and any potential relationship between agricultural emissions and NPF events. A field campaign was conducted for 3 months at the FR-Gri-ICOS site (France), at an experimental farm 25 km west of Paris city centre.

16 NPF events have been identified from the analysis of particle number size distributions; 8 during the daytime, and 8 during the night-time. High solar radiation and ozone mixing ratios were observed during the days NPF occurred, suggesting photochemistry plays a key role in daytime NPF. These events were also associated with higher levels of VOCs such as isoprene, methanol, or toluene compared to non-event days. However, ammonia levels were lower during daytime NPF events, contributing to the hypothesis that daytime NPF events were not related to agricultural activities.

On the other hand, temperature and ozone were lower during the nights when NPF events were observed, whereas relative humidity was higher. During these nights, higher concentrations of NO_2 and ammonia were observed. As a result, agricultural activities, in particular the spreading of fertilizer on surrounding crops, are suspected to contribute to night-time NPF events.

Finally, all the identified NPF events were also observed at SIRTA monitoring station 20 km from the FR-Gri ICOS site, showing that both night-time and daytime NPF events were regional

processes. We hypothesise that night-time NPF may be related to fertilizer spreading over a regional scale, as opposed to the local activities at the farm. To our knowledge, this is the first time night-time NPF has been observed in the agricultural context.

Keywords: New Particle Formation, Agriculture, Air quality, Ammonia, VOCs

Graphical abstract

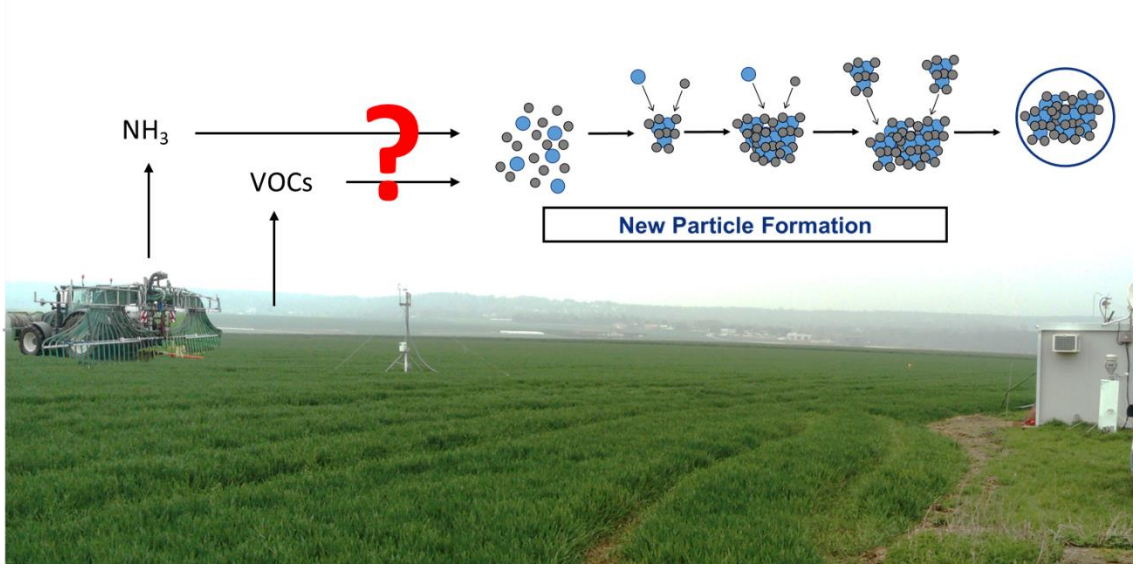

1. Introduction

Atmospheric particles are widely recognised as strongly affecting both air quality and climate. In the last AR5 report, the IPCC (International Panel for Climate Change) evaluated that interactions of atmospheric particles with solar radiation and clouds were still one of the greatest uncertainties in the evaluation of the Earth's radiative forcing budget (IPCC, 2021). New particle formation (NPF) is the secondary process by which particles are generated in the atmosphere, from the gas-particle conversion of extremely low volatility vapours. Several studies have already highlighted that NPF is a significant source of atmospheric particles, and can be a major contributor to cloud condensation nuclei (CCN) in different locations worldwide (Merikanto et al., 2009; Rose et al., 2014; Wang et al., 2017).

NPF generally occurs through two steps: the nucleation, which is initiated by the formation of a stable clusters from gaseous species; and the growth, the activation of these clusters followed by a subsequent growth, which implies the condensation of low volatility vapours. The first step, *i.e.* nucleation, consists of the formation of stable clusters, ranging from a few molecules to up to more than 10 molecules (Andreae, 2013). Currently, it is assumed that nucleation is mostly based on sulfuric acid clusters formed with other gaseous species, such as water, ammonia (NH_3), or extremely low volatility organic compounds – ELVOCS - (Berndt et al., 2014; Kulmala et al., 2014). There is also evidence that clusters are formed from NO_3^- ions and highly oxidised molecules (HOMs), especially at night, when sulfuric acid concentrations are lower (Bianchi et al., 2019; Rose et al., 2018). A laboratory study evidenced nucleation from the oxidation of pure biogenic volatile organic compounds (BVOCs), meaning that BVOC oxidation products are able to produce stable clusters without the presence of inorganic ions (Kirkby et al., 2016). Several field studies have reported the involvement of BVOCs in NPF when combined with other gases, but evidence of pure biogenic nucleation has only been demonstrated in laboratory experiments (Bianchi et al., 2019; Debevec et al., 2018; Kammer et al., 2020; Rose et al., 2018). The second step, the growth, is

associated with the coagulation of the smallest particles and the condensation of low to extremely low volatility compounds such as HOMs that are produced from the oxidation of biogenic or anthropogenic volatile organic compounds (VOCs) (Bianchi et al., 2019; Wang et al., 2017). The growth step is essential if the particles are to reach a diameter where they can act as CCN.

NPF has been observed in various locations worldwide, e.g. in urban environments, in the free troposphere, in remote boreal forests, tropical environments, coastal sites, etc. (Alam et al., 2003; Kanawade et al., 2022; Kerminen et al., 2018; Kulmala et al., 2004; Wang et al., 2017; Xiao et al., 2021; Young et al., 2013; Yu et al., 2020). This process is also known to occur not only locally, but also at regional levels (Kerminen et al., 2018; Kulmala et al., 2012; Wehner et al., 2007). In urban environments, NPF events are often related to environmental parameters, such as solar radiation, but also air mass history and properties, including precursor gas concentrations, and the atmospheric particle loading (Dall'Osto et al., 2013b; Dunn et al., 2004; Hakala et al., 2022; Kanawade et al., 2012; Nilsson et al., 2001; Salma et al., 2011; Stanier et al., 2004; Wonaschütz et al., 2015). The presence if pre-existing particles favours the condensation of low volatility gases, leading to a competition between condensation and nucleation processes. NPF under conditions of high particle loading has also been reported, in particular in developing countries such as China and India, due to the very high concentration of precursors in the air. This emphasizes the variety of conditions under which NPF can occur (Huang et al., 2016; Kanawade et al., 2022; Wang et al., 2017; Xiao et al., 2015; Yu et al., 2017). The balance between low volatility gases and pre-existing particles is thus one of the elements in determining the occurrence of NPF. It is clear that sulfuric acid is involved in NPF in urban environments, but it cannot explain alone the intensity of the observed NPF events. Thus, it is proposed that photochemistry of anthropogenic VOCs, especially those resulting from biomass burning, could be involved in NPF in urban environments, but this has not been clearly demonstrated so far (Wang et al., 2017). Considering the prevalence of nitrogen

oxides in the urban environment, NO_3^- based clusters might also play a significant role in urban NPF.

NPF has been mostly reported during the daytime and related to photochemical processes, notably to the formation of sulphuric acid. However, a few studies have reported night-time events, mainly in remote areas, and rarely in urban areas (Junninen et al., 2008; Kammer et al., 2018b; Kecorius et al., 2015; Lee et al., 2008; Ortega et al., 2012; Salimi et al., 2017; Svenningsson et al., 2008; Vehkamaki et al., 2004). For night-time events, the sulphuric acid based nucleation scheme is not likely to explain night-time NPF, as sulphuric acid production is related to photochemistry (Kammer et al., 2018b; Lee et al., 2008; Ortega et al., 2012). Previous studies have suggested that monoterpene ozonolysis can contribute to the initiation of nocturnal events observed at forest sites, but it has yet to be demonstrated. Overall, it is clear that our current understanding of NPF mechanisms is still incomplete.

A recent review regarding NPF observations noted the lack of studies detailing NPF in agricultural areas, as only one study has been recently published regarding NPF at a mixed coastal/agricultural site (Kerminen et al., 2018; Olin et al., 2022). Indeed, agriculture covers around a third of land area according to the Food and Agriculture Organization of the United Nations (http://www.fao.org/faostat/en/#data/RL, last access September 2022). Yet, agriculture is the main source of NH_3 on a global scale (Behera et al., 2013), a molecule known to catalyse nucleation by clustering with sulphuric or nitric acids (Aksoyoglu et al., 2020; Berndt et al., 2014; Lehtipalo et al., 2018). NH_3 emissions from crop fields are related to the spreading of fertilisers, such as manure or slurry. Organic fertilisers also emit a wide variety of VOCs into the atmosphere, including carboxylic acids (e.g. butyric acid, acetic acid), aromatics (e.g. phenol, methyl phenol), nitrogen containing VOCs (e.g. dimethylamine, indole) and sulphur containing VOCs (e.g. methanethiol, dimethylsulfide) (Behera et al., 2013; Feilberg et al., 2015; Liu et al., 2018; Parker et al., 2013; Potard et al., 2017; Woodbury et al., 2014). Amines emitted by the application of organic fertilisers

are reported to be highly efficient clustering molecules (Chee et al., 2019; Ciuraru et al., 2021; Schobesberger et al., 2013; Yao et al., 2018). A few studies also showed that sulphur containing compounds such as dimethylsulphide or methane sulphonic acid may be involved in NPF processes (Berndt et al., 2014; Schobesberger et al., 2013; Xu et al., 2020). Thus, considering the nature of the VOCs emitted during the spreading of organic fertilisers, there is clearly a strong potential for NPF formation in agricultural areas, especially during organic fertiliser spreading periods.

In this context, the present study is aimed at investigating NPF in relation to agricultural activities at a peri-urban agricultural site. It consisted of *i*) identifying the presence (or absence) of NPF, *ii*) highlighting the meteorological and physico-chemical conditions favouring NPF, *iii*) evaluating a potential relationship between agricultural emissions and NPF, and iv) an assessment of whether NPF is a local or regional process.

2. Materials and methods

2.1. Experimental set-up

The field campaign was part of the AgriMultiPol programme funded by the French Environment and Energy Management Agency (ADEME n°17-03 C0012). The study was conducted from March 13th 2018 to May 9th 2018, at the FR-Gri ICOS field site (48.84 N, 1.95 E, 125 m above mean sea level), in the Grignon experimental farm, which combines crops and livestock (https://www.fermedegrignon.fr/). The field campaign was conducted on a 20 ha crop field of winter wheat at its growth stage, on a soil that can be classified as luvisol. The site is located 25 km west of Paris city centre, and near the city of Plaisir (*ca*. 31 000 inhabitants), which is situated to the south of the site, heavily trafficked roads surround the east and south sides of the farm (**Figure S1 and S2**). Dairy and sheep buildings are positioned to the southwest of the farm (**Figure S1**). VOC and NH_3 emissions as well as the composition of particles from the farm have been characterised in a previous study (Kammer et al., 2019). The prevailing air masses is expected to come from the west-south-west, originating from the Atlantic Ocean. The field site is part of the

European Research Infrastructure ICOS (FR-Gri-ICOS, Integrated Carbon Observation System) and has been previously described in detail elsewhere (Loubet et al., 2012, 2011; Stella et al., 2013). Several agricultural practices were carried out during the field campaign: mineral fertilizer was spread on March 16th 2018, liquid manure on March 29th 2018, a fungicide on April 17th 2018, and an herbicide on the contour of the field on May 5th 2018.

2.2. Sampling and instrumentation

To investigate NPF, particle number size distribution (PNSD) was measured using a scanning mobility particle sizer (SMPS, TSI, model 3080). This instrument has been used in numerous studies and already fully described elsewhere (Kammer et al., 2018b; Kulmala et al., 2012). Briefly, the instrument consists of a long differential mobility analyser (DMA, TSI model 3082) and a water-based condensation particle counter (CPC, TSI model 3768). Ambient air was sampled at 0.6 L min^{-1} through a 1.8 m long conductive silicon tubing (4.5 mm inner diameter), above the shelter at 3 m above ground level. In this configuration, the instrument was able to characterise the PNSD with an electrical mobility diameter between 4.6 nm and 156.8 nm. The sampled air was not dried, to avoid any modification to its size, due to evaporation of semi volatile material and water. Condensation in the line and the instrument cannot be completely ruled out, but was not expected as the SMPS, was located in a temperature-controlled shed, and the residence time in the line was very short (0.9 s). In addition, the sample relative humidity measured by the instrument never reached more than 66 % (sample relative humidity at SMPS inlet). More, RH was below 90 % most of the time (over 93 % of the time during the campaign), and 94 % of temperatures were below 20 °C, while the inside temperature was maintained at least at 20 °C during the campaign. In addition, high temperatures coincided with low relative humidity, leading to the conclusion that condensation was unlikely to happen. Leak checks were performed twice a week throughout the campaign using a high efficiency particle filter (HEPA filter, TSI) placed at the inlet of the instrument. Particle losses inside the tubing have been estimated based on the methodology proposed by Willeke and

Baron (1993). The highest loss rates were found to be around 45 % for the finest size ranges measured by the SMPS (*i.e.* particles with an electrical mobility diameter of 4.6 nm). The PNSD measured by the SMPS has thus been corrected to take these losses into account.

Meteorological parameters were measured from a mast located at the centre of the crop field, as part of the ICOS network (ICOS level 2 station). Wind speed and directions were recorded using a 2-dimensional sonic anemometer (Wind Sonic, GILL), and air temperature and relative humidity using a probe (HMP155 Vaisala). Solar radiation was measured as photon photosynthetic flux density (PPFD) using a pyranometer (CMP22, Kipp & Zonen). Friction velocity (u* in m s^{-1}) can be used as proxy to represent the intensity of turbulence in the atmosphere, which was derived from 3D-sonic anemometer measurement (Wind Sonic, GILL). All the meteorological measurements were monitored at 5 m above ground level and were recorded at 10 min time intervals using a data logger (CR1000, Campbell scientific).

NH_3 concentrations have been measured using a laser-based photoacoustic detector (LSE Monitors B.V.). The air was sampled using 1.2 m long Teflon tubing (⅛ inches diameter) at a flow rate of 0.040 L min^{-1}. The main inlet was heated at 40/45 °C to prevent condensation, and a Teflon filter was used to avoid particles penetrating into the instrument. The NH_3 analyser was calibrated before the campaign and had a detection limit of 1 ppb (1 standard deviation), one data point was recorded every minute.

VOCs were also measured using a proton transfer reaction – quadrupole ion guide – time of flight – mass spectrometer (PTR-Qi-TOF-MS, Ionicon), that has been extensively described previously (Abis et al., 2018; Gonzaga-Gomez et al., 2019; Loubet et al., 2021). The air was sampled at 1.8 m above ground level at 50 L min^{-1} through 30 m Teflon tubing (½ inch diameter) using a Busch SV-1010 pump (Busch, SW), and was regulated using a mass flow controller (Bronkhorst). The air was sub-sampled by the PTR-Qi-TOF-MS at 0.3 L min^{-1}, using a 1 m long PFA tube (⅛ inches diameter). The pressure in the drift tube was regulated at 4±0.0001 mbar at a temperature of 80±0.06

°C, and a drift voltage of 996.5±0.5 V. These conditions in the drift tube ensured an E/N ratio (where E is the electric field strength and N the gas number density) of 132±1 Td (1 Td = 10^{-17} V cm^{-2}), which has been reported to be a good compromise to between sensitivity variations due ambient humidity changes, and high fragmentation (Pang, 2015; Tani et al., 2003). Blanks were frequently performed using zero air (Alphagaz 1, zero air: 80% nitrogen, 20% oxygen, purity: 99.9999%, Air Liquide), and the instrument sensitivity during the campaign was evaluated using a toluene gas standard (102±10 ppb, Messer), following the methodology described in Kammer et al. (2019).

2.3. Measurements at SIRTA monitoring station

PNSD were measured simultaneously with another SMPS at the SIRTA (Site Instrumental de Recherche par Télédétection Atmosphérique, http://sirta.ipsl.fr) monitoring station, which is part of the EU ACTRIS (Aerosols, Clouds, and Traces gases Research InfraStructure Network, http://www.actris.net) research infrastructure. SIRTA is a monitoring station located 20 km south of the Paris metropolitan area (48.71◦N, 2.15◦E, , 150 m above sea level), and 20 km to the south east of the Grignon field site (see **Figure S2**), and has been described extensively in numerous previous studies (see for example, Haeffelin et al. (2005)). At SIRTA, the PNSD was recorded with an SMPS (GRIMM, model 5416), measuring electrical mobility diameters from 10 to 500 nm. As at the FR-Gri-ICOS site, the sample was not dried, and leak checks were frequently performed throughout the campaign using a HEPA filter (TSI).

3. Methodology

3.1. NPF event detection and classification

NPF events were identified through visually inspection of the PNSD following the method described by Dal Maso et al. (2005): an NPF event was defined as a clear increase in the particle concentration in the nucleation mode, followed by a growth during at least two hours producing the

well-known “banana shape” (Dal Maso et al., 2005; Heintzenberg et al., 2007). Then, to analyse the environmental factors driving NPF at the FR-Gri-ICOS site, we classified days according to the presence or absence of NPF (event days or non-event days). A third category of weak event and/or growth days was also defined, when NPF was suspected but the banana shape could not be clearly differentiated from the growth of pre-existing particles, or when the PNSD was too heavily loaded to clearly identify the banana shape. These days were termed “undefined” days. Days were classified as:

- NPF event days: a clear NPF was identified
- Undefined days: a weak NPF and/or a growth was identified
- Non-event days: no NPF was identified

The same classification has been performed for nights, as NPF events were recorded during both nights and days during the field campaign. In this study, days are defined as periods when solar radiation (*i.e.* the PPFD in this study) is over 50 µmol m^{-2} s^{-1} (and nights when it is below this threshold). This corresponds to daytime period typically from 7:00 to 17:00 UTC (8:00 to 18:00 local time) for the first days of the campaign, and typically from 5:00 to 18:00 UTC (7:00 to 20:00 local time) at the end of the campaign. Night-time periods are thus typically from 17:00 to 7:00 UTC (18:00 to 8:00 local time) for the first days of the campaign, and typically from 18:00 pm to 5:00 UTC (20:00 to 7:00 local time) at the end of the campaign.

3.2. Characterisation of NPF events

The potential loss of semi volatile vapours on existing particles could be estimated by calculating the condensation sink (CS) as in (Dal Maso et al., 2005; Kulmala et al., 2001):

$$CS = 4\pi D \sum_i \beta_{Mi} r_i N_i \quad (1)$$

Where CS is the condensation sink (in s^{-1}), D is the diffusion coefficient of the condensing vapour (assimilated here to sulphuric acid, D is 0.14 cm^2 s^{-1}), β_{Mi} is the transitional correction factor, r_i is the mobility radius of particles (in cm) taken from the measured PNSD by the SMPS, and N_i is the particle concentration (in particles cm^{-3}) in the size bin i. The transitional correction factor was computed as:

$$\beta_{Mi} = \frac{Kn+1}{0.377 + 1 + \frac{4}{3}\alpha^{-1}Kn^2 + \frac{4}{3}\alpha^{-1}Kn} \quad (2)$$

Where α is the sticking coefficient (assumed to be 1, as recommended by Kulmala et al. (2001)) and Kn (unitless) is the Knudsen number computed as:

$$Kn = \frac{\lambda_v}{r_i} \quad (3)$$

Where λ_v (in cm) is the mean free path.

NPF events could be characterised by the growth rate (the speed at which particles grow during the event) and the nucleation rate of particles. The growth rates (GR, in nm h^{-1}) have been calculated at each time step following the maximum concentration method described by Kulmala et al. (2012):

$$GR = \frac{\mathrm{d}D_p}{\mathrm{d}t} \quad (4)$$

Where D_p is the geometrical mean diameter of the nucleation mode (in nm), and $\mathrm{d}t$ is the measurement time step (in s). D_p was obtained for each PNSD event, by identifying the diameter corresponding to the maximum concentration of particles in the nucleation range (particles with an electrical mobility diameter < 25 nm) (Kulmala et al., 2012).

The nucleation rate (J_{nuc} in particle cm^{-3} s^{-1}) is defined as the flux of newly formed particles in the nucleation size range, here taken as particles with a diameter less than 25 nm (electrical mobility diameter) (Hussein et al., 2005; Jaatinen et al., 2009; Seinfeld and Pandis, 2006). The estimation of

the nucleation rate during NPF events is based on the description of the evolution of the particle population, as a function of its sources and sinks:

$$J_{nuc} = \frac{dN}{\mathrm{dt}} + F_{coag} + F_{growth} \quad (5)$$

Where $\frac{dN}{\mathrm{dt}}$ is the evolution of particle concentration in the nucleation mode (particles with an electrical mobility diameter < 25 nm) as a function of time (assuming that the only source of particles is from nucleation, in particle cm^{-3} s^{-1}), F_{coag} is the loss of particles due to coagulation in the nucleation size range (in particle cm^{-3} s^{-1}) and F_{growth} the growth of particles to sizes larger than the nucleation range (in particle cm^{-3} s^{-1}). The $\frac{dN}{\mathrm{dt}}$ term in the equation can be directly estimated from SMPS measurements:

$$\frac{dN}{\mathrm{dt}} = \int_{Dp_{min}}^{25} n_N(D_p).dD'_p \quad (6)$$

With Dp_{min} the minimum diameter measured by the SMPS (electrical mobility diameter 4.6 nm) and $n_N(D_p)$ is the measured PNSD in the nucleation range. F_{growth} has been estimated following the methodology described by Kulmala et al. (2012):

$$F_{growth} = GR(D_p).n_N(D_p) \quad (7)$$

where GR is the growth rate of particle over the nucleation range estimated based on equation 4. Then, F_{coag} is estimated as (Hussein et al., 2008; Kulmala et al., 2012) :

$$F_{coag.} = CoagS_{nuc}N_{nuc} \quad (8)$$

Where $CoagS_{nuc}$ is the coagulation sink (in cm^3 s^{-1}) over the nucleation range expressed as:

$$CoagS_{nuc} = \int_{D'_{p1}}^{D'_{p2}} K(D_pD'_p).n_N(D_p).dD'_p \quad (9)$$

Where $K(D_pD'_p)$ (in cm^3 s^{-1}) is the coagulation coefficient of 2 particles of diameters D_p and D'_p, calculated following Fuchs (1964).

4. Results

4.1. General conditions of the campaign

During the field campaign, the average air temperature was 10.8 °C, with a minimum temperature of -2.4 °C and a maximum of 26.7°C, and relative humidity varied between 100 % and 24 %, covering a wide range of atmospheric conditions. The climate was largely under the influence of the Atlantic Ocean, as about half of the air masses originated from west-south-west. Air masses from the east-northeast were downwind from the Paris urban area and central European continent, and generally presented higher concentrations of NO_x, as illustrated by the NO_2 pollution rose (**Figure 1.a**). This is supported by NO_2 maps of the Ile de France region that have been generated through modelling or from satellite measurements, clearly marking the Paris area and roads as NO_2 hotspots (**Figure S2**). During the campaign, NO and NO_2 were on average 1.1 ppb and 5.6 ppb, respectively, but reached values up to 48 ppb and 34 ppb for NO and NO_2, respectively. High NO concentrations could be associated road traffic, due to the proximity of roads, especially to the east of the field site, which can be subject to heavy traffic loads during morning and evening rush hours (**Figure S2**).

The site was located inside the vicinity of the Grignon experimental farm, which combined crops and livestock (dairy and sheep). VOCs, particles and NH_3 emissions from the farm buildings have been characterised in previous studies (Kammer et al., 2019; Loubet et al., 2012). More generally, the measurement site was in an agricultural region dominated by crops with little livestock. The influence of agricultural activities on the gas phase chemical composition have been evaluated through the measurement of NH_3. Concentrations of NH_3 were on average 13.4 ppb and ranged from the detection limit of the instrument (1 ppb) up to 42.8 ppb. The highest levels of NH_3 were recorded during the first half of the campaign that usually corresponded to a period of fertilizer application on crops on a regional level. As the atmospheric lifetime of NH_3 is rather short (from a few hours to a day, depending on conditions), its atmospheric concentration is mainly driven by

emissions. Mineral and organic (bovine sludge) fertilizers were applied to the measurement site on March 17th 2018 and March 29th 2018 respectively. Both spreading induced an increase in NH_3 concentrations but did not correspond to the measured maximum of NH_3 (**Figure S3**). The highest concentration of NH_3 was observed on the April 1st 2018, four days after the spreading of bovine sludge on the field site. The delay can be explained by i) rain events following the application and ii) sources other than the local spread fertilizers, such as activities at the surrounding fields. More, a long trend increase of NH_3 was observed from March 20th 2018 until April 10th 2018, where the concentration remained above 10 ppb, suggesting a higher NH_3 background concentration. This increase over a long time period suggests that in addition to local applications, regional sources affected the ambient NH_3 levels at the measurement site. This is confirmed by the NH_3 pollution rose showing contributions from all wind directions at both low and high wind speeds (**Figure 1**). In particular, the direction of the farm does not necessarily correspond to the highest concentration of NH_3. More, NH_3 did not seem to be favoured neither by high nor low wind speed (**Figure 1**). As a conclusion, sources responsible for high NH_3 levels cannot be solely attributed to the agricultural activities at the farm. The contribution of other surrounding fields where fertilizer had been spread, or even at larger scale probably contributed to the observed increase in NH_3 during the first half of the campaign.

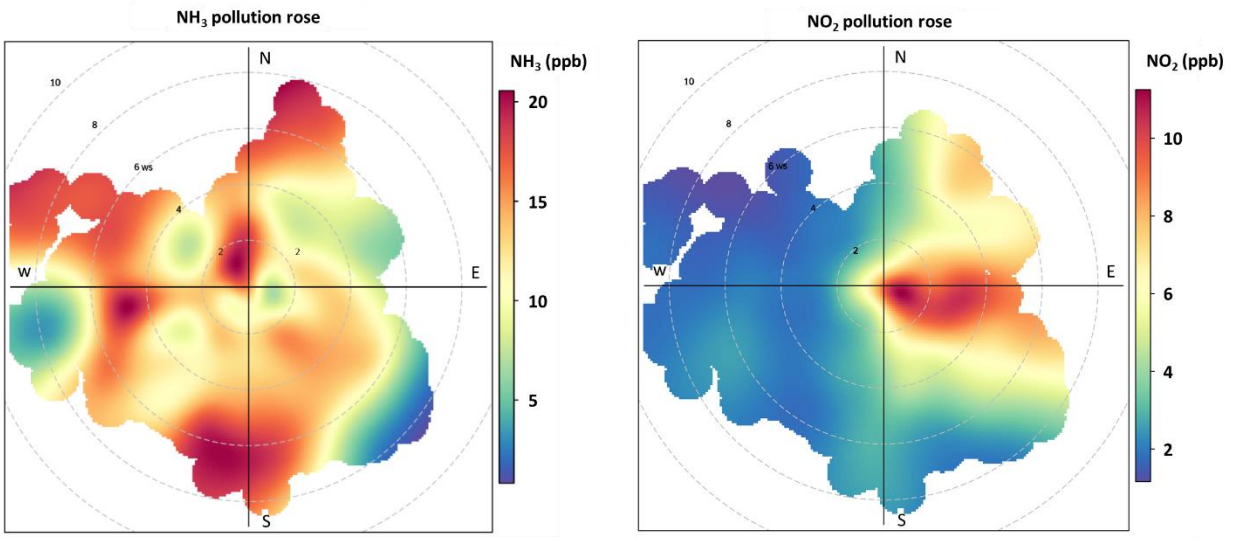

Figure 1: Pollution roses of NH_3 (in ppb, left panel) and NO_2 (in ppb, right panel).

PNSD was measured during the campaign at FR-Gri-ICOS and simultaneously at SIRTA station, 20 km away. The location of the 2 sites regarding Paris area can be seen on **Figure S2**. The PNSD at both sites present many similarities despite the instruments measuring slightly different particle size ranges (**Figure S3**). At both sites, the particle modes were generally centred between 50 nm and 100 nm. The PNSD from FR-Gri-ICOS site was more loaded than the SIRTA one, probably due to its proximity to the particle sources, in particular traffic roads nearby the site. However, it seems that many events observed from the PNSD measurements at one site can also be observed at the other one. A more in-depth comparison of the PNSD and NPF events at the 2 sites is provided in section 4.5.

4.2. NPF events

During the field campaign, a total of 16 NPF events were identified according to the classification described in **section 3.1**. All the identified NPF events and several parameters characterising the NPF are listed in **Table 1**. Two types of NPF events were observed. The first type of event occurred during the daytime: the nucleation phase typically started in the morning, then particles grew during the following daylight hours and lasted until the end of the day, or even into the hours of darkness for a few NPF events (events 9, 11, 16). These events correspond to typical regional daytime events frequently reported in the literature in remote as well as urban areas (Dal Maso et al., 2005; Kerminen et al., 2018; Kulmala et al., 2004; Lee et al., 2019). For the second type of event NPF was initiated in the evening, around sunset (just before or just after), and the following growth period occurred during the night and ended before sunrise. In the following parts of the manuscript, these second type of events will be referred as night-time events as they mostly took place during the hours of darkness. A typical example of each type (daytime and night-time) of event is provided in **Figure 2,** and examples of undefined and non-event days are provided in **Figure S4**. Among the 16 events, 8 occurred during daytime and 8 have been classified as night-time events (**Table 1**).

The occurrence of nocturnal events is not common as most studies report only daytime events, mostly related to photochemistry (Lee et al., 2019; Lehtipalo et al., 2018). The few studies reporting night-time events were in remote forested sites such as an Eucalyptus forest in Australia (Suni et al., 2008) or a pine forest in France (Kammer et al., 2018b). Only one study has reported nocturnal NPF events at an urban site (Salimi et al., 2017). **Figure 2** illustrates a clear difference between daytime and night-time events, particularly in the shape of the NPF plots. During the initiation of NPF events, the increase in the particle concentration at the lowest particle size range (between 5 and 10 nm electrical mobility diameter) was shorter in duration for night-time compared to daytime events. This could be the result of a lower particle formation rate for night-time NPF events due to specific conditions at night (higher humidity, less wind, …). Another possibility is that NPF was initiated earlier in the air mass and had been transported to the FR-Gri-ICOS site later, meaning that the initial steps of NPF were missed. The sharp increase in the lowest particle mode was also reported for night-time events in a previous study, but this cannot be generalised to all NPF night-time events, as only a few are reported in the literature (Kammer et al., 2018a).

During the campaign, daytime events occurred mainly during the second half of the campaign, whereas night-time events were mainly observed during the first half of the campaign (**Table 1**). GR were generally higher for night-time (average GR of 5.3 nm h^{-1}) than for daytime NPF events (average GR of 3.4 nm h^{-1}). This is illustrated from the growth of particles to a larger diameter during the night-time event represented in **Figure 2**. The calculated GR are in line with previous studies conducted in suburban areas where GR are typically in the range 1-10 nm h^{-1} (Chu et al., 2019; Kulmala et al., 2004; Salimi et al., 2017; Zhu et al., 2013). The GR of night-time events were slightly lower than those reported in forested areas, but are in agreement with GR reported for night-time events in Brisbane, Australia by Salimi et al. (2017).

Average nucleation rates were in the same range for both daytime and night-time events, with average values of 63 particles cm^{-3} s^{-1} and 52 particles cm^{-3} s^{-1}, respectively. However, nucleation rates for night-time events seemed to be more variable than for daytime events. (**Table 1**). The range of observed nucleation rates are comparable to previous studies (when calculated using the same size range), even if it seems slightly higher than some studies in comparable peri-urban environments (Chu et al., 2019; Hussein et al., 2008; Jaatinen et al., 2009; Wu et al., 2007).

NPF events were reported for both continental and oceanic air masses, as well as different wind directions including from the east, which corresponds to Paris area (**Figure S2 and S11**).

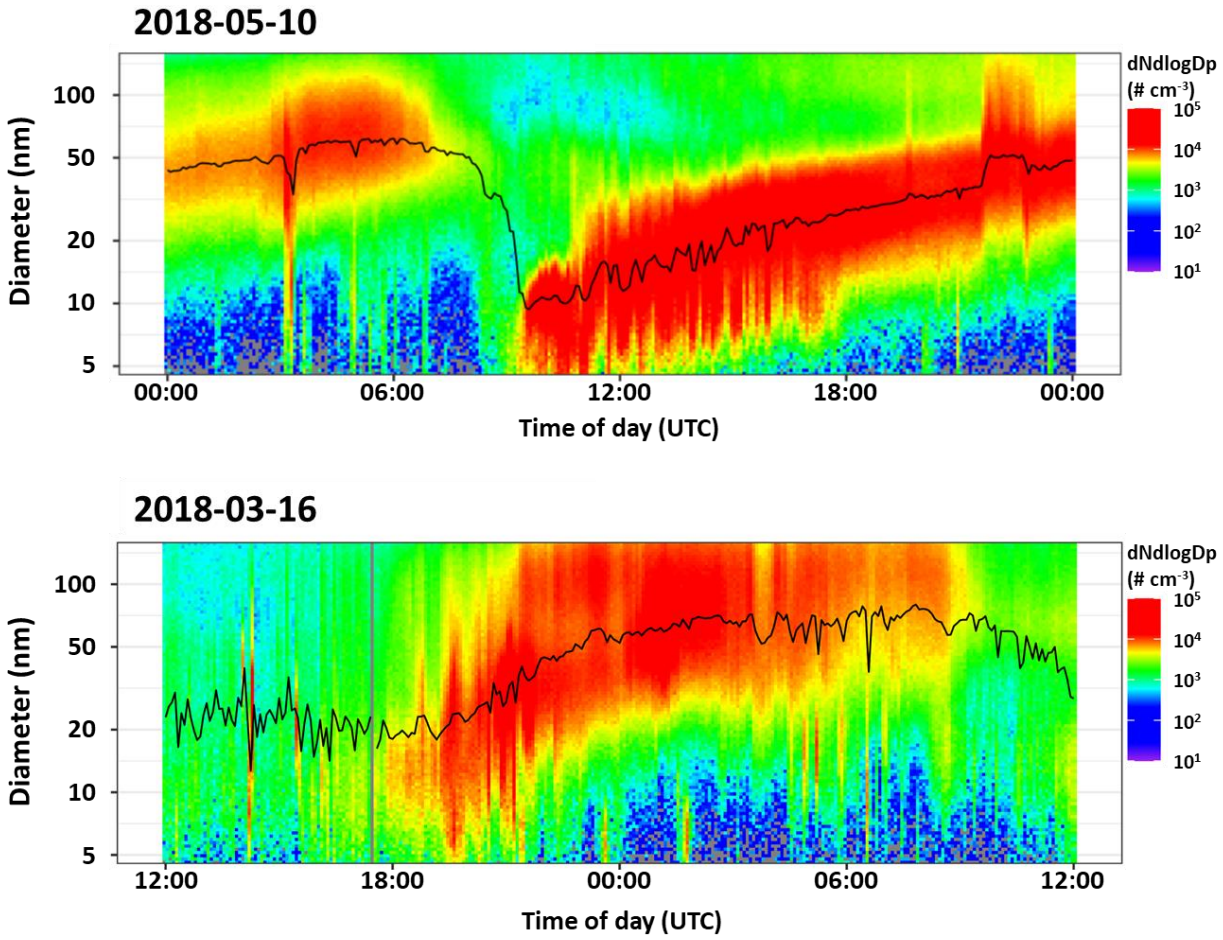

Figure 2 : Typical example of new particle formation events observe at the FR-Gri ICOS measurement station. The top panel represents a daytime NPF event, whereas the bottom panel refers to a night-time NPF event. The grey bar on the night-time panel (just before 18:00) corresponds to missing data due to a leak check.. The black line represents the median mode diameter of the particles After March 25th 2018, local time was switched from UTC+1hto UTC +2 (due to the switch from French winter to summer time).

Table 1: List of NPF events start and end times, type of event (gold = Daytime, blue = Night-time), and the corresponding mean growth rate (GR) and nucleation rate (J). The condensation sink (CS), the air temperature (T), the relative humidity (RH), the wind speed (WS) and the friction velocity (u*) are reported for NPF start time. After March 25th 2018, local time was switched from UTC+1h, to UTC +2 (due to the switch from French winter to summer time).

Event n°	Start date (UT)	End Date (UT)	CS ($\times 10^{-3}$ s^{-1})	GR (Nm h^{-1})	$\frac{CS.10^4}{GR}$	J (cm^{-3} s^{-1})	PPFD µmol m^{-2} s^{-1}	T (°C)	RH (%)	WS (m s^{-1})	u* (m s^{-1})
N1	2018-03-13 17:00	2018-03-14 04:00	7.2	4.4	16	120	65	10.5	64	3.3	NA
N2	2018-03-15 17:00	2018-03-16 01:00	5.0	4.4	11	9	140	10.1	78	4.0	NA
N3	2018-03-16 18:00	2018-03-17 08:00	10.1	6.7	15	37	8.5	8.8	70	3.3	NA
N4	2018-03-24 19:00	2018-03-25 07:00	33.6	4.1	82	63	0	10.7	55	0.9	NA
N5	2018-03-30 16:00	2018-03-31 03:00	2.2	5.1	4	18	413	8.3	67	4.0	0.37
N6	2018-04-03 17:00	2018-04-04 01:00	4.9	4.1	12	12	267	10.4	78	3.5	0.36
N7	2018-04-05 17:30	2018-04-06 02:00	14.6	4.6	32	145	139	9.2	49	1.13	0.15
N8	2018-04-08 18:30	2018-04-09 03:00	12.0	9.0	13	8	66	17.0	47	3.5	0.29
Average	**17:30**	**03:30**	**11.2**	**5.3**	**23.1**	**52**	**137.3**	**10.6**	**63.5**	**3.0**	**0.3**
D1	2018-04-04 09:00	2018-04-04 19:00	3.1	2.2	14	54	880	11.4	68	4.4	0.36
D2	2018-04-17 10:00	2018-04-18 03:00	8.4	3.8	22	48	1357	16.2	49	3.4	0.36
D3	2018-04-22 11:00	2018-04-22 17:00	9.8	3.4	29	19	1527	23.3	42	3.8	0.16
D4	2018-04-26 08:00	2018-04-27 04:00	4.4	2.1	21	48	758	9.5	71	4.3	0.33
D5	2018-04-28 10:30	2018-04-28 16:00	5.2	2.7	19	34	809	12.8	56	4.8	NA
D6	2018-05-07 11:00	2018-05-07 16:00	18.0	6.0	30	41	1717	23.4	31	3.6	0.34
D7	2018-05-09 09:00	2018-05-09 13:00	10.4	4.3	24	160	1283	14.6	69	2.6	NA
D8	2018-05-10 09:00	2018-05-11 08:00	4.0	2.3	17	100	659	11.9	66	4.8	NA
Average	**09:40**	**00:00**	**7.9**	**3.4**	**22.0**	**63.0**	**1123.8**	**15.4**	**56.5**	**4.0**	**0.3**

NA: Not-Available.

388

Thus, air mass origin has no effect on the occurrence of either daytime or night-time NPF, contrary to what was observed elsewhere (Kim et al., 2019, 2016; Salimi et al., 2017; Wonaschütz et al., 2015). This result is surprising because NPF was not expected to occur when air masses were affected by emissions from Paris urban area, as NPF is known to be favoured by clean air masses. The plume from the Paris urban area usually had a higher particle loading (compared to air masses of oceanic origin), leading to a higher condensation sink (CS) competing with NPF processes. This is confirmed by the pollution rose of the CS, showing that highest levels of CS were observed to an easterly direction, similar to the NO_2 pollution rose, and also for lower wind speeds suggesting local sources of particles (**Figures 1 and S5**). The relation between NO_2 and CS is clearly visible in **Figure S6**.

NPF in polluted air masses has already been observed in urban areas, especially in Chinese megacities (Chu et al., 2019; Wang et al., 2017). It is worth noting that even if CS values were higher when associated with the Paris plume, they remained lower than what has been reported for Chinese megacities (Chu et al., 2019). As a result, NPF events occurred in polluted plumes as well as clean oceanic air masse, indicating that one or several factors other than CS were limiting NPF at the FR-Gri-ICOS site. The ratio of GR to CS can be used as a parameter to estimate the occurrence of NPF (Chu et al., 2019; McMurry et al., 2005). Except for some studies in highly polluted environments, it has been shown that NPF does not occur when GR/CS is higher than 50 (Chu et al., 2019). The results presented here mostly conform to NPF occurring when CS/GR is lower than 50, even for night-time events, as only one exception was found on the night from March 24th 2018 to Marche 25th 2018(**Table 1**).

4.3.Daytime NPF and photochemistry

To investigate the driving parameters of daytime NPF, the diurnal trends resulting from the classification detailed in **section 3.1** are presented in **Figure 3**. First, as expected, the CS was lower for category 1 (corresponding to NPF days) at the NPF start time (from 08:00 to 11:00). The CS

then increased during the day due to the formation and growth of the particles (**Figure 3**). The difference between clear and undefined days was quite small because, as explained above, NPF sometimes occurred with high values of CS when the air mass was affected by Paris urban area emissions, and undefined days corresponded to situations when NPF was not clearly defined and potentially situations where many diameters of the PNSD were highly concentrated.

Daytime NPF events were clearly characterised by higher temperatures and higher solar radiation, in agreement with previous studies (Kulmala et al., 2004). This supports the theory that nucleation is triggered by sulphuric acid cluster formation, as sulphuric acid production is directly dependent on photochemistry (Andreae, 2013; Kulmala, 2003). In addition, more photochemistry results in higher concentrations of oxidants (mostly OH radicals and O_3 during daytime), and greater production of a wide variety of species that can be involved in NPF such as extremely low volatility oxidation products or nitric acid (Bianchi et al., 2016; Chee et al., 2019; Hakala et al., 2019). Photochemically induced NPF explains why daytime NPF events were observed during the second half of the campaign, as solar radiation increased as the campaign progressed (**Figure S2** and **Table 1**).

Interestingly, the time of NPF initiation varied quite a lot (**Table 1**). We noted that late start events were associated with higher values of CS or lower solar radiation (**Table 1**). This is even clearer in **Figure S7**, which represents the event start date as a function of solar radiation and CS. When CS was high, NPF initiation was delayed because of the competition between condensation and nucleation. Hence, later in the day due to the enhanced photochemistry, more condensable vapours were produced and nucleation became more favourable despite the higher CS. Similarly, when PPFD was lower, the photochemistry was less intense, and the time for key species such as sulphuric acid to reach the supersaturation concentration was longer.

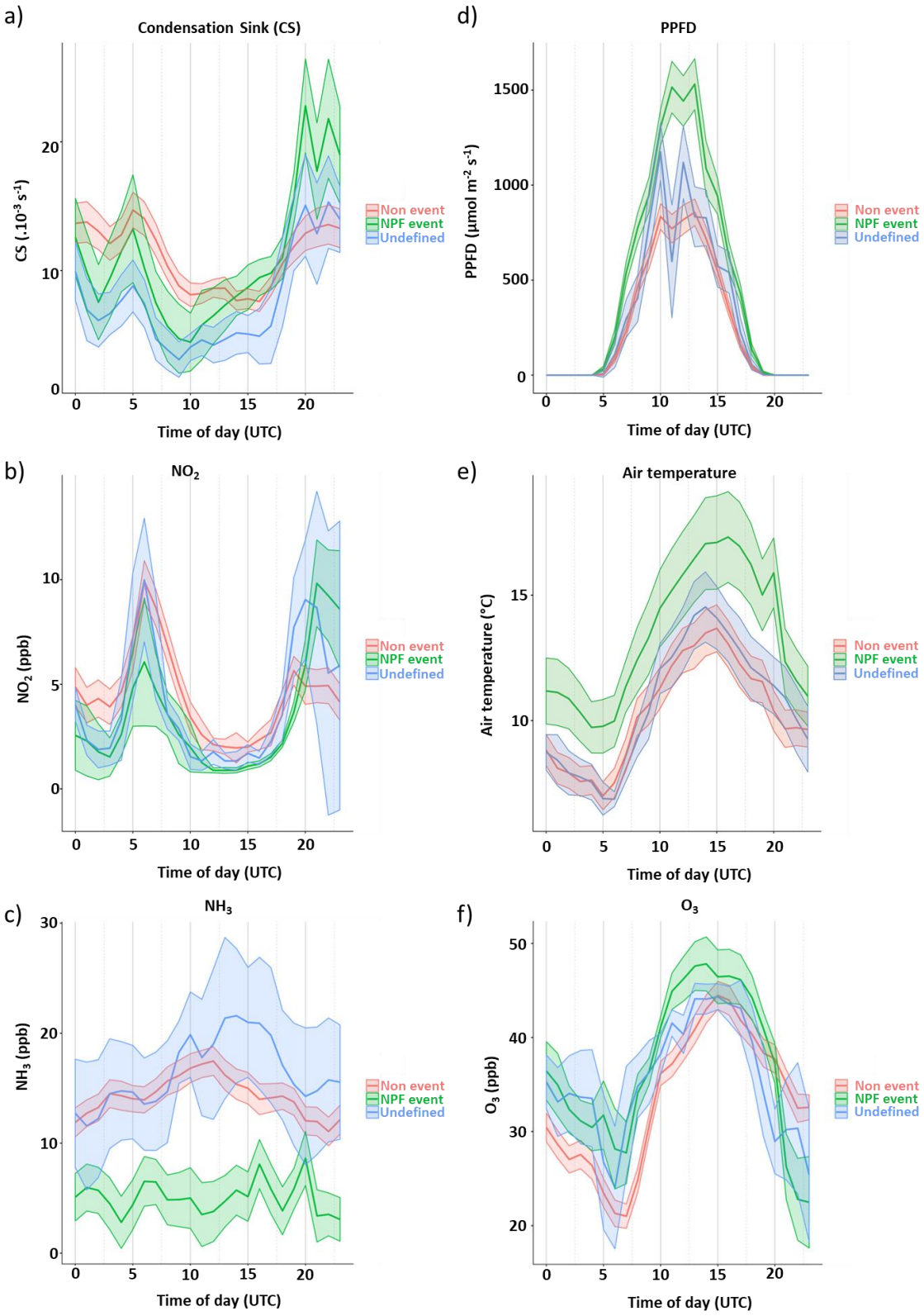

Figure 3: Diurnal profiles of a) condensation sink (CS, in s^{-1}); b) NO_2 (in ppb), c) NH_3, d) Photosynthetic Photon Flux Density (PPFD, in W m^{-2}), e) air temperature (in °C) and f) O_3 (in ppb) as a function of NPF categories. For each graph, the colored line and shaded area indicate mean and standard error, respectively, for NPF (green), non-event (red) and undefined (blue). After March 25th 2018, local time was switched from UTC+1h, to UTC +2 (due to the switch from French winter to summer time).

NO_2 levels were also lower during NPF days, there are 2 main reasons for this. First, the observation of low NO_2 during NPF days means that polluted air masses did not favour NPF. Thus, although analysis of air masses performed above showed that NPF events sometimes occurred in air masses influenced by Paris urban area emissions, it seems that they only happened when the plume was not highly polluted (highly loaded with NO_2 and particles). The second reason is the higher solar radiation observed during NPF days lead to higher photolysis of NO_2, causing its concentration to decrease. In conclusion, the lower NO_2 observed during NPF days can be explained by lower emissions and higher photolysis. Regarding NPF, it supports the importance of photochemistry and the weak contribution of anthropogenic emissions to daytime NPF observed at FR-Gri-ICOS site.

Ozone concentrations were also higher on the days NPF occurred, strengthening the hypothesis that daytime NPF was induced by photochemistry, in agreement with higher NO_2 photolysis (**Figure 3**). The consequence of stronger photochemistry is that more oxidation products can be produced due the reaction of organic species with atmospheric oxidants, such as ozone or OH radicals. To check this hypothesis, we analysed the concentrations of gaseous precursors (i.e., VOCs).

Methanol (CH_4O, measured at m/z 33.033) and isoprene (C_5H_8, measured at m/z 69.070) are typically associated with biogenic emissions (Gonzaga-Gomez et al., 2019; Kesselmeier and Staudt, 1999). The isoprene concentration was pretty low, with an average concentration of 0.16±0.1 ppb. These generally low isoprene levels could be a favourable condition for NPF as a high level of isoprene has been reported to supress NPF in certain conditions (Kanawade et al., 2011; Kiendler-Scharr et al., 2009). In this study, both isoprene and methanol were more concentrated during NPF days compared to non-NPF days (**Figure 4**), potentially meaning there were more oxidation products during NPF days (note that even if methanol is not a precursor of low volatility products, it is used here as tracer for biogenic emissions). However, isoprene and methanol presented an unusual diurnal trend. Isoprene is recognised as mainly being emitted by trees, shrubs and grass, while methanol is the main VOC emitted by crops (including the soil) (Bachy et al., 2020; Gonzaga

Gomez et al., 2019; J Kesselmeier and Staudt, 1999; Laothawornkitkul et al., 2009). Considering the context of the field site (peri-urban agricultural site), methanol can be reasonably attributed to the surrounding crops, while forests are likely sources of isoprene, but whether these species originated from local or regional sources depends on atmospheric transport (Bachy et al., 2020; Loubet et al., 2021). As biogenic emissions are related to solar radiation and temperature which peak around midday, methanol and isoprene emissions reach their maximum in most rural areas at this time (Cai et al., 2021; Gentner et al., 2014; Graus et al., 2013). In our study, isoprene and methanol presented unusual night-time maxima, increasing in the evening around 20:00 UTC, this trend was even more pronounced during NPF event days (**Figure 4**). We hypothesise that these daily patterns resulted from the combination of a ground-based emissions during the night and the building of the stable nocturnal boundary layer (reducing the height of the atmospheric mixing layer), as already observed in forested areas for VOCs emitted during dark hours (Kammer et al., 2018b). In addition, their pollution roses are quite similar and pointed to 2 sources; a regional one to the east, in addition to a strong local contribution, more visible on the isoprene pollution rose (**Figure S8**). More, methanol and to a lesser extent isoprene show an exponential relation with air temperature (**Figure S9**), but no relation to solar radiation (not shown). Such behaviour has been observed for soil emissions at agricultural sites, and can indicate that the local source of methanol might be the soil of the FR-Gri-ICOS site and surrounding crop stands **(**Bachy et al., 2018**)**.

More, both methanol and isoprene have similarities with the NO_x diurnal cycle (*i.e.*; increase at evening around 20:00 UTC) and pollution rose, to the relation is stronger with NO_2 than with NO (**Figures 3, 4 and S8**), suggesting a contribution of anthropogenic sources such as residential solid fuel burning or traffic. This is supported by the similar trend (evening increase) and pollution rose of toluene, also pointing in an easterly direction (**Figures 4 and S8)**, usually attributed to anthropogenic sources (Bruns et al., 2017; Languille et al., 2020). More precisely, the diurnal cycle is typical of field sites strongly influenced by biomass burning, with a large evening peak, then

decreasing, with a short peak appearing in the evening (Chazeau et al., 2021; Dall'Osto et al., 2013a). A noticeable pattern was the spike observed in methanol mixing ratios in the morning that may be attributed to methanol evaporation with dew (Bachy et al. 2018) although it could also be linked with traffic. The second option may be the most plausible as the same morning peak is observed for the NO_2 diurnal trend (**Figure 3**).

Methyl vinyl ketone (MVK, C_4H_6O) and methacrolein (MACR, C_4H_6O) are two gas phase oxidation products resulting from isoprene photooxidation, and are used as markers of photochemical activity (Paulot et al., 2009). As these compounds are isomers, they were both detected at m/z 71.084 by the PTR-Qi-TOF-MS (de Gouw and Warneke, 2007). The concentration of MVK+MACR was rather low (below ppb level) but was higher in the mornings of NPF daytime events (i.e. when NPF is initiated). One can suppose that this result supports the importance of photochemistry to daytime NPF. However, their daily pattern was expected to present higher concentrations during the daytime, in relation to photochemistry. In our case, especially during NPF days, the concentrations of the sum MVK+MACR peaked in the evening and during early morning, suggesting that photochemical production of MVK+MACR is unlikely. We thus propose that another isomer was probably contributing to the signal at this m/z, or another source of these compounds contributed to their signal.

More advanced analysis (such as positive matrix factorization, PMF) of the various source contributions to ambient VOC levels would be helpful to understand the dynamics of VOC concentrations at the measurement site, but identification and quantification of VOC sources is beyond the scope of the present paper.

Finally, a potential relation to agriculture was investigated using NH_3 as a tracer for agricultural emissions. **Figure 3** shows that the levels of NH_3 were clearly lower on NPF days compared to non-NPF days. This was expected considering that daytime NPF mostly occurred during the second half of the campaign, whereas the period corresponding to organic fertiliser spreading was the first

half of the field campaign. As a result, we can reasonably hypothesise that observed daytime NPF events at the FR-Gri-ICOS site were not associated with high NH_3 concentrations and agricultural emissions, even this cannot be completely ruled out. We suggest that daytime NPF was rather linked to photochemistry, in agreement with previous studies.

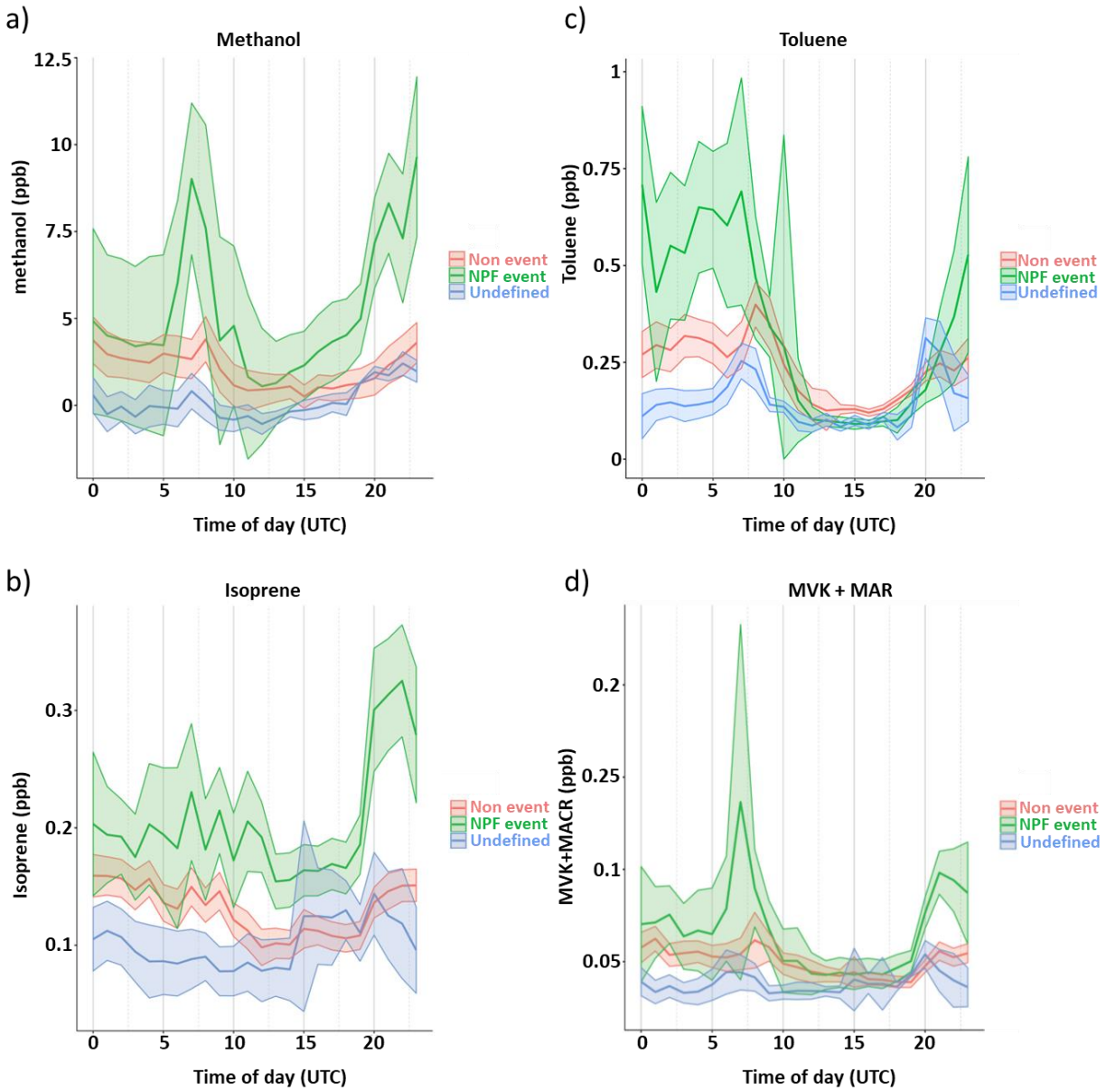

Figure 4: Diurnal profiles of a) methanol (m/z 33.033, in ppb); b) isoprene (m/z 69.070, in ppb), c) toluene (m/z 93.070, in ppb) and d) the sum of methyl vinyl ketone and methacrolein (MVK+MACR, m/z 71.048, in ppb) as a function of NPF categories. For each graph, the colored line and shaded area indicate mean and standard error, respectively, for NPF (green), non-event (red) and undefined (blue). After March 25th 2018, local time was switched from UTC+1h, to UTC +2 (due to the switch from French winter to summer time).

4.4. Parameters driving night-time NPF

As explained in section 3.1, night-time NPF events differed from daytime events in several ways. Similar to the analysis performed for daytime events, nocturnal trends of the different physico-chemical and meteorological parameters have been investigated in relation to the presence (or absence) of night-time NPF events (**Figure 5**). First, we observed that on the nights when NPF events occurred, the CS was lower at NPF start time (between 16:00 and 19:00 UTC, **Figure 5**). Then, CS increased through the night due to the formation of particles and their growth throughout the night, as was observed for daytime NPF events. The CS was slightly higher for night-time undefined events (at NPF start time), meaning that during these nights there was competition between NPF and condensation processes. As expected, air temperature was lower for NPF nights (**Figure 5**), because they were identified during the first part of the field campaign, and logically, relative humidity was thus higher during NPF nights (**Figure S10**). Surprisingly, wind speed was not a meaningful factor for night-time NPF (**Figure 5**), contrary to what was reported in previous night-time NPF studies (Kammer et al., 2018). The values of u* (**Table 1**) support the hypothesis that the building of a night-time stable boundary layer was not a prerequisite for NPF (nocturnal profiles are not represented due to a significant amount of missing data, especially during NPF nights), despite some data being missing. This is also strengthened by investigating the Monin–Obukhov length (a key parameter for atmospheric stability, Irwin and Binkowski, 1981), which indicates that the stable nocturnal layer was not a necessity for night-time NPF. Previous studies on night-time NPF evidenced that a stable atmosphere (induced by lower wind speed) is required to trigger NPF (Kammer et al., 2018b; Kecorius et al., 2015; Man et al., 2015). The building of the stable nocturnal boundary layer coincides with a drop in wind speed and, as a result, a lower dilution of ground-based emissions (that are concentrated within a smaller surface layer). Thus, the resulting increase in concentration of low volatility gases helps them to reach their super saturation ratio. In our case, wind speed reached up to 4 m s^{-1} when night-time NPF started (Table 1) and was always

higher than 0.9 m s^{-1} (**Table 1**). This is supported by the analysis of the friction velocity. Thus, the precursor gases present at the initiation of night-time NPF did not require a reduced boundary layer to reach supersaturation. This result suggests that night-time NPF at FR-Gri-ICOS was not related to ground-based emissions.

NO_2 concentrations were high on the nights when clear and undefined NPF occurred (category 1 and 2) compared to non-event nights (**Figure 5**). High NO_2 concentrations are associated with high CS values, especially for night-time conditions (**Figure 5**). This explains why NO_2 was also high for clear and undefined nights, as the undefined NPF events might have corresponded to the nights when a high CS prevented a clear banana shape event. As NO_2 is usually associated with anthropogenic emissions, its higher concentration might indicate that anthropogenic emissions were involved in night-time NPF. We therefore, examined the nocturnal trend of the BTEX (Benzene, Toluene, Ethylbenzene and xylenes), recognised as tracers of anthropogenic sources (Jiang et al., 2017). The toluene nocturnal trend is represented in **Figure 6** as an example of trend for BTEX species. The toluene concentration was not higher at the time of night-time NPF initiation but was higher after midnight. It means that anthropogenic VOCs might be involved in the growth steps of night-time NPF, as precursors of condensable vapours. Higher NO_2 levels during NPF and undefined nights could alternatively mean higher concentrations of NO_3 radicals as the oxidation of NO_2 is the main source of NO_3 radicals (especially due to the reaction with O_3). On one hand, higher NO_3 levels means more oxidation of VOC precursors leading to higher concentrations of low volatility species that can be involved in NPF. On the other hand, it can also lead to the formation of ammonium nitrate (NH_4NO_3) in the particle phase. For example, Man et al. (2015) showed in a field study in Korea that NH_4NO_3 was involved in the growth stage of NPF. Gas to particle conversion of NH_4NO_3 has been observed by Nemitz et al. (2009) after fertilisation over grassland, but has not been associated with NPF events. In summary, high concentrations of NO_2 during NPF nights may suggest that two processes are involved in night-time NPF: gas to particle

conversion of NH_4NO_3 and condensation of low volatile gases resulting from VOC oxidation by NO_3 radicals.

As explained O_3 could be involved in NO_3 formation through the oxidation of NO_2. We observed that O_3 concentrations were lower during NPF nights (**Figure 5**). As O_3 is a secondary compound from photooxidation, it is reasonable to consider that there is no source of O_3 during dark hours. Thus, the lower values of O_3 might be an indication of higher consumption, either due to physical (*i.e*. deposition) or chemical sinks. As ozone surface deposition is mostly driven by turbulence (Kammer et al., 2018a; Potier et al., 2015), it cannot explain the lower O_3 concentrations observed during NPF nights, as there was no difference in wind speed during these nights. We finally assume that lower O_3, during NPF nights, implies a higher consumption by chemical reactions, potentially with NO_2 that would support the importance of NO_3 in NPF.

The nocturnal trend of NH_3 by category of nights supports the hypothesis of the importance of NH_4NO_3 in night-time NPF, as NH_3 levels were higher during the nights when NPF events were identified (**Figure 5**). This is in line with the period when night-time NPF occurred (first half of the campaign), that typically corresponded to a period of intensive fertiliser spreading in the Ile de France region (Fortems-Cheiney et al., 2020). The higher humidity and lower temperatures during NPF nights are 2 environmental factors favouring gas-particle partitioning of NH_4NO_3 toward the particle phase. NH_4NO_3 has been shown to efficiently participate in aerosol growth after grassland fertilisation (Nemitz et al., 2009). In addition to the formation of NH_4NO_3, NH_3 is also reported to catalyse NPF by stabilising clusters in the very first steps of NPF (*i.e.* nucleation) (Almeida et al., 2013; Schobesberger et al., 2013). Thus, the role of NH_3 in NPF could be both through the formation of NH_4NO_3 and the formation of stable clusters. The role of NH_3 has already been highlighted in the field by different studies, but is always associated with daytime events and ternary nucleation of $NH_3/H_2SO_4/H_2O$ (Birmili and Berresheim, 2003; Größ et al., 2018; Xiao et al., 2015).

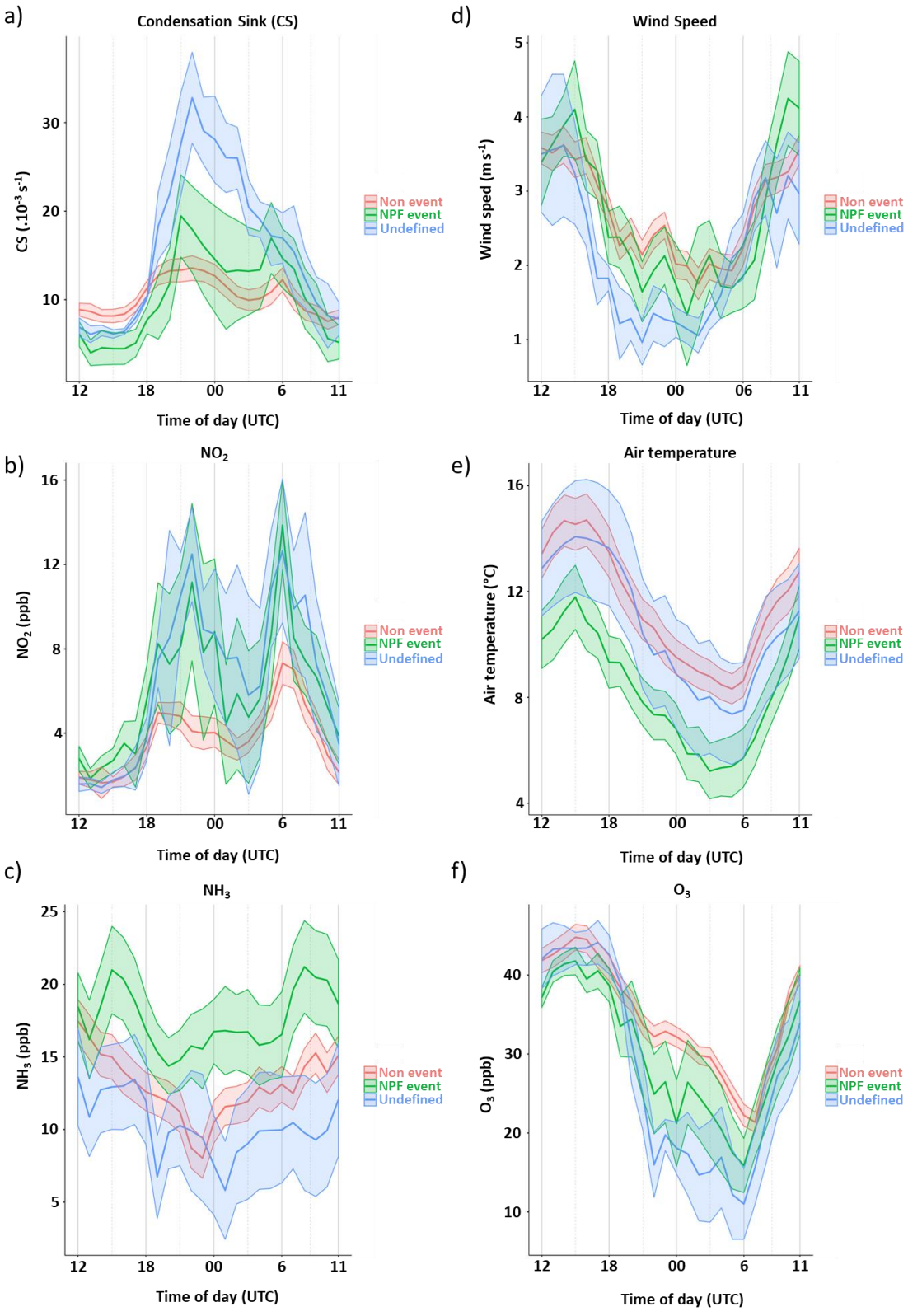

Figure 5: Diurnal profiles of a) condensation sink; b) NO_2, c) NH_3, d) wind speed, e) air temperature and f) O_3 as a function of night-time NPF categories. For each graph, the colored line and shaded area indicate mean and standard error, respectively, for NPF (green), non-event (red) and undefined (blue). After March 25th 2018, local time was switched from UTC+1h, to UTC +2 (due to the switch from French winter to summer time).

In this case, it is very unlikely that the classical ternary nucleation involving H_2SO_4 triggered the observed NPF, as H_2SO_4 formation is mostly related to photochemical reactions. One possibility is that other acids, such as organic acids that can be emitted by fertilisation activities, participate in the nucleation steps. Then, the condensation of NH_4NO_3 can explain the growth, as Nemitz et al. (2009) estimated that it can induce growth rates of 11 nm diameter particles from 1 to 7 nm h^{-1} over a grassland in Germany, which is typically in the range of the GR measured at FR-Gri-ICOS site. In the end, the mechanism by which NH_3 promotes NPF in our study is still unclear and requires further investigation. Finally, considering the agricultural character of the field site and the period of night-time NPF, we can attribute the higher levels of NH_3 to the agricultural spreading of organic fertilizer. Thus, we can reasonably hypothesise that the occurrence of night-time NPF in spring at FR-Gri-ICOS was related to fertiliser spreading.

As NPF night-time events were observed during the first half of the campaign, it is expected that they were not related to higher biogenic emissions, contrary to what was observed for daytime NPF events. This is confirmed by investigating the nocturnal cycle of biogenic VOCs, such as methanol that was clearly lower during NPF nights (**Figure 6**). VOCs typical of agricultural activities and organic fertiliser spreading were also investigated, even if their emissions are not well characterised thus far. Most of VOCs were less concentrated on the nights we identified NPF events. For example, trimethylamine (C_3H_9N, m/z 60.081) is known to be emitted from fertilizer spreading (Liu et al., 2018; Potard et al., 2017; Woodbury et al., 2014) and to catalyse NPF (Duporté et al., 2016; Yao et al., 2018), but was not higher during NPF nights (**Figure 6**).

The only VOC that was clearly higher during NPF nights (compared to non NPF nights) was acetic acid, that is also reported as an organic fertiliser emission (**Figure 6**) (Liu et al., 2018; Potard et al., 2017; Woodbury et al., 2014). Its concentrations were also high during undefined nights. Thus, acetic acid might be one of the contributors to night-time NPF events, among other parameters such as pre-existing particle loading (*i.e.* condensation sink) in determining whether NPF happened or

not. Acetic acid has been reported to enhance nucleation through the stabilisation of clusters, similar to NH_3 (Nadykto and Yu, 2007; Zhu et al., 2014). In addition, this acid can undergo reactions with different bases including NH_3. A higher acetic acid concentration could thus favour the condensation of NH_3. The contribution of acetic acid would imply agricultural emissions played a role in night-time NPF, but a more comprehensive study regarding the chemical composition of aerosols at the molecular scale will be necessary.

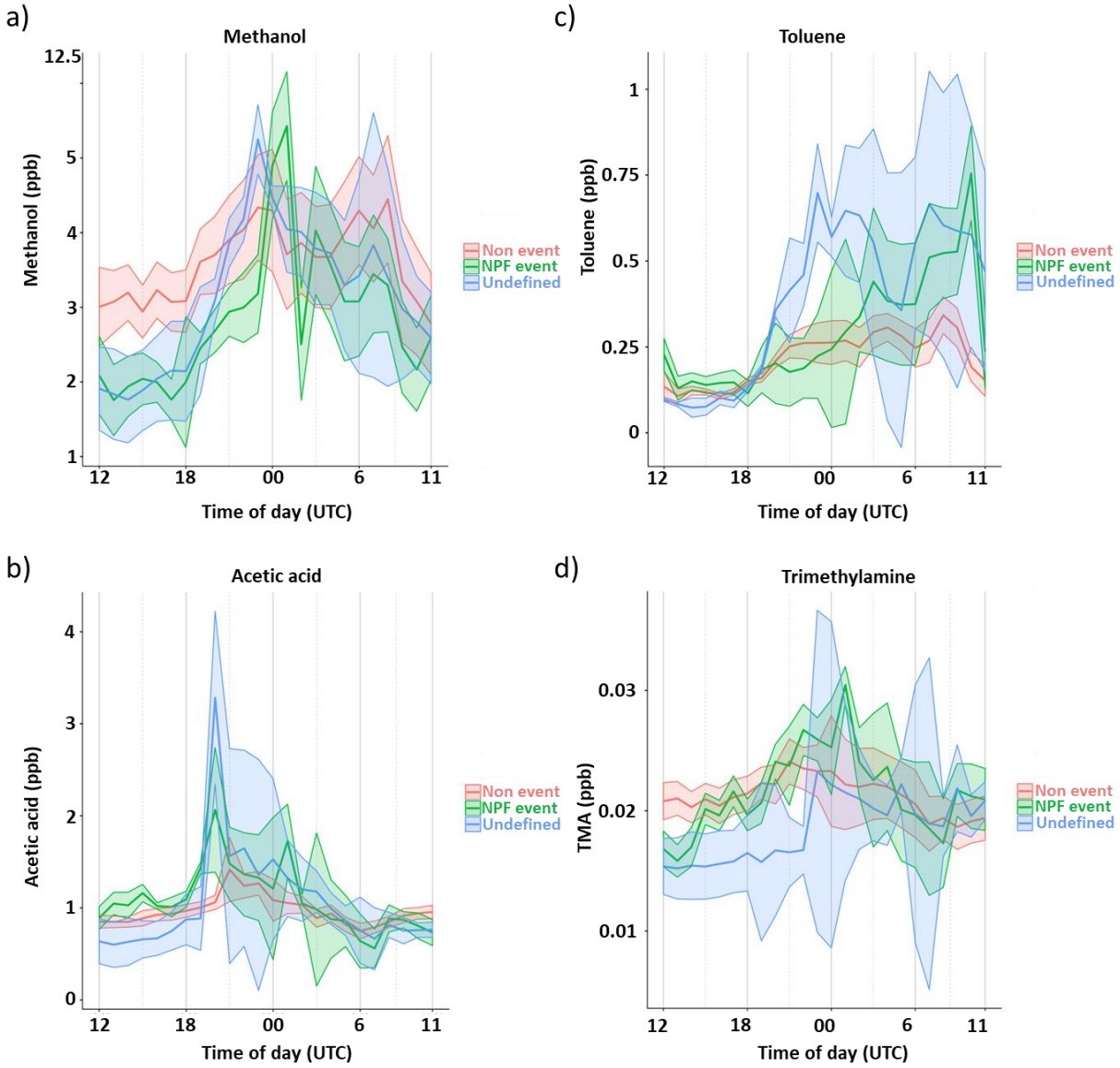

Figure 6 : Diurnal profiles of a) methanol (m/z 33.033, in ppb), b) acetic acid (m/z 61.028, in ppb), c) toluene (m/z 93.070, in ppb) and d) trimethylamine (m/z 60.081, in ppb) as a function of night-time NPF categories. For each graph, the colored line and shaded area indicate mean and standard error, respectively, for NPF (green), non-event (red) and undefined (blue). After March 25th 2018, local time was switched from UTC+1h, to UTC +2 (due to the switch from French winter to summer time).

4.5. Are night-time NPF events regional?

We also investigated whether the observed NPF events were regional phenomena by comparing the PNSD obtained at the FR-Gri-ICOS site to the one from the SIRTA site, 20 km away. The methodology described in **section 3.1** was also applied to identify NPF events from PNSD measurements at the SIRTA station. First, all the NPF events observed at FR-Gri-ICOS were also observed at the SIRTA site. This result was expected for daytime NPF events, that are clearly defined as a regional process based on the numerous studies available in the literature (Kerminen et al., 2018; Kulmala et al., 2004). However, less is known about night-time NPF events, and we show here that night-time events also occurred on a regional scale. It means that the parameters driving night-time NPF were probably more regional than local. As a result, if agricultural emissions were involved in the night-time NPF observed, it was related to the fact that the Ile de France region, and more precisely the footprint area of NPF; has a high density of crops, and that farmers usually spread fertilisers during the same time period. Then, even if farmers do not spread the same types of fertilizers on the same days, a large scale spreading over typically a 1- or 2-week period creates a large source of NH_3 that may last for several weeks after the initial spreading. This is supported by the high NH_3 background concentrations during the first half of the field campaign, and the pollution rose of NH_3 showing contributions from all wind directions (**Figures 1 and S3**). This phenomenon can explain both the regional phenomena of night-time NPF and the link with agriculture. However, this theory must be confirmed through further investigations. The importance of meteorological parameters is strengthened by the fact night-time NPF is regional, as they are generally similar at a regional scale. In the case of night-time NPF, we highlighted the importance of both temperature and relative humidity, while it is still hard to disentangle the effect of each parameter, respectively.

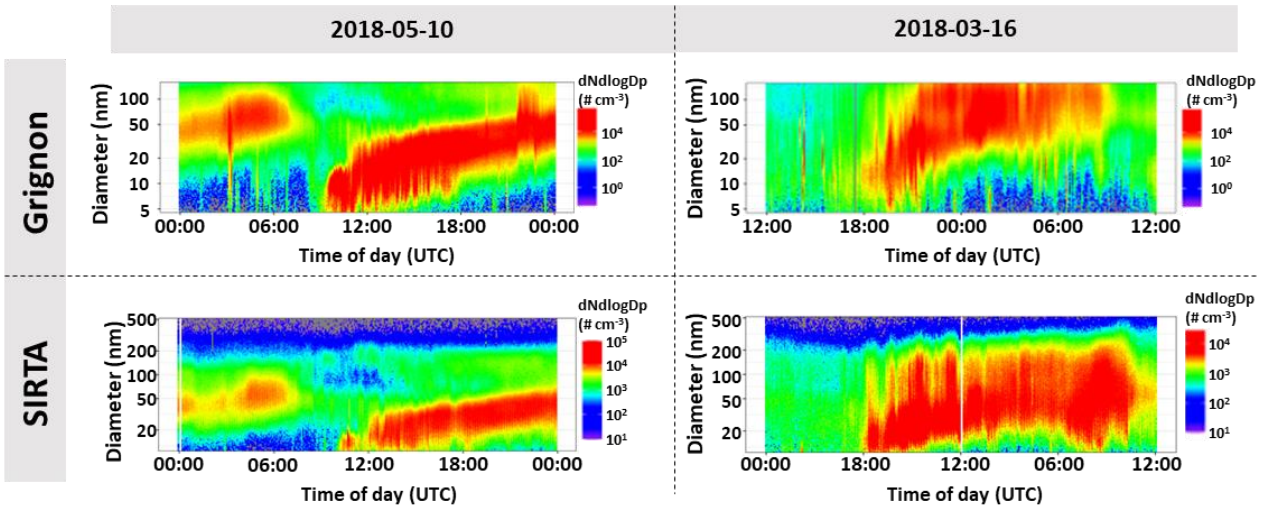

Figure 7: Typical example of new particle formation events observed at the FR-Gri ICOS measurement station and at the same time at the SIRTA station. The top panels represent events at FR-Gri ICOS and bottom panels at SIRTA. Left panels represent a daytime NPF event, whereas right panels show a night-time NPF event. Note that Y scales are different for top (Grignon) and bottom (SIRTA) plots, due to different SMPS configurations for measuring PNSD. After March 25th 2018, local time was switched from UTC+1h, to UTC +2 (due to the switch from French winter to summer time).

We then compared the start time of each event at each site. Generally, no lag time was observed for night-time NPF events despite the difference in the lower diameter of the two instruments, and the distance between the two sites. In contrast, the start times of daytime events were not the same for each daytime NPF event. This lag time was not constant and varied from half an hour up to 2 hours (**Table 2**). The onset of NPF events appeared always earlier at FR-Gri-ICOS, except for 1 event (event n° 13, **Table 2**). Wind speed values at NPF start time, reported in **Table 2**, were used to evaluate if the simple displacement of the air mass from one site to the other could explain the observed lag time for daytime NPF. No relation can be observed between the wind speed and the lag time. In addition, daily airmass backward trajectories have been computed for both sites for the entire campaign (**Figure S11**). Analysis of the resulting backward trajectories first showed that the same air mass was sampled at both FR-Gri-ICOS and SIRTA sites. Moreover, it seemed clear that there was no relation between the origin of the air mass and the lag time of NPF events. Even for the only event when NPF started earlier at SIRTA compared to FR-Gri-ICOS, no specific air mass

origin was observed (**Figure S11**). More studies are thus needed to fully understand the factors driving NPF events observed at both sites, and more generally in peri-urban agricultural areas.

Table 2: List of NPF events start times at both FR-Gri-ICOS and SIRTA. Wind speeds (WS) at FR-Gri-ICOS NPF event start time are provided to evaluate the potential relation between the evolution of the air mass and the lag time in NPF start time (UTC) between the 2 sites.

Event n°	Date	Time start at FR-Gri-ICOS (UTC)	Time start at SIRTA (UTC)	WS ($m\ s^{-1}$)
1	2018-03-13	17:00	17:00	3.3
2	2018-03-15	17:00	17:00	4.0
3	2018-03-16	18:00	18:00	3.3
4	2018-03-24	19:00	19:00	0.9
5	2018-03-30	16:00	16:00	4.0
6	2018-04-03	17:00	17:00	3.5
7	2018-04-04	09:00	11:00	4.4
8	2018-04-05	17:30	17:30	1.13
9	2018-04-08	18:30	18:30	3.0
1ß	2018-04-17	10:00	11:00	3.4
11	2018-04-22	11:00	12:00	3.8
12	2018-04-26	08:00	09:00	4.3
13	2018-04-28	10:30	10:00	4.8
14	2018-05-07	11:00	12.00	3.6
15	2018-05-09	09:00	10:00	2.6
16	2018-05-10	09:00	10:00	4.8

5. Conclusion

A field campaign has been conducted within the Grignon experimental farm, which is a peri-urban agricultural site located at 25 km west of Paris city centre. 16 NPF events have been identified, 8 NPF events during the daytime and 8 during the night-time. GR and nucleation rates were in the range of reported values, for both daytime and night-time events. Daytime events were observed during the second part of the campaign, when solar radiation and ozone concentrations were higher. They are thus proposed to be related to photochemical processes in agreement with previous

studies. As NH_3 concentrations were lower on the days NPF was observed, we supposed that daytime NPF was not related with agricultural activities.

In contrast, night-time NPF events occurred during the first half of the campaign and were associated with low temperatures and high relative humidity. They were associated with higher NH_3 levels suggesting that they might be related to agricultural emissions, and more specifically to fertiliser spreading. We hypothesised that high NH_3 levels were due to both local and regional sources and cannot be solely explained by the agricultural practices that happened on the field site during the campaign. The processes at the initiation of night-time NPF were thus probably not local, but rather regional suggesting that meteorological conditions were important NPF drivers.

The NPF events observed at the FR-Gri-ICOS site were also detected at a the SIRTA monitoring station located 20 km to the southeast. This confirms that daytime NPF events were regional processes, as previously reported in different studies, and showed for that night-time NPF events were also regional. In conclusion, there appears to be a potential relation between night-time NPF and agriculture, due to regional agricultural activities rather than local fertiliser spreading. We suggest that the spreading of fertilisers by numerous farmers in the Ile de France region in the same time period could explain the relation between agriculture and night-time NPF. However, a more extensive study is needed to fully elucidate this. In addition, more studies detailing NPF in other regions in the world with intense agriculture would be necessary to verify whether the results obtained in this study can be extended to other agricultural areas.

Acknowledgments: Yves Python and Dominique Tristant are thanked for providing access to experimental farm. The authors acknowledge ANAEE-France for the PTR-Qi-TOF-MS funding, and the French Environment and Energy Management Agency ADEME for the funding through the AgriMultiPol program (17-03 C0012). This work was performed at the ICOS FR-Gri level 2 site, which is part of the ICOS (Integrated Carbon Observatory System) European Research

Infrastructure. All the authors greatly acknowledge Hayley Furnell (University College Cork) for the help in the English revision of the manuscript.

Competing interests: The authors declare no competing of interest.

Data and materials availability:

All the data used in this article are publicly available at the following address https://doi.org/10.57745/XMPAVS (last access September 2022) and can be identified using the corresponding doi 10.57745/XMPAVS.

Author contribution

JK designed and performed field measurement, analysed the data and wrote the manuscript. LS analysed SMPS data and revised the manuscript. RC, JEP, FL, PB, SB, BH, SC, OF and FT participated in the field campaign and revised the manuscript. VG and BL created the AGRIMULTIPOL project, designed the field campaign, participated in field campaign and revised the manuscript.

References

Abis, L., Loubet, B., Ciuraru, R., Lafouge, F., Dequiedt, S., Houot, S., Maron, P.A., Bourgeteau-Sadet, S., 2018. Profiles of volatile organic compound emissions from soils amended with organic waste products. Science of The Total Environment 636, 1333–1343. https://doi.org/10.1016/j.scitotenv.2018.04.232

Aksoyoglu, S., Jiang, J., Ciarelli, G., Baltensperger, U., Prévôt, A.S.H., 2020. Role of ammonia in European air quality with changing land and ship emissions between 1990 and 2030. Atmospheric Chemistry and Physics 20, 15665–15680. https://doi.org/10.5194/acp-20-15665-2020

Alam, A., Shi, J.P., Harrison, R.M., 2003. Observations of new particle formation in urban air. Journal of Geophysical Research: Atmospheres 108. https://doi.org/10.1029/2001JD001417

Almeida, J., Schobesberger, S., Kürten, A., Ortega, I.K., Kupiainen-Määttä, O., Praplan, A.P., Adamov, A., Amorim, A., Bianchi, F., Breitenlechner, M., David, A., Dommen, J., Donahue, N.M., Downard, A., Dunne, E., Duplissy, J., Ehrhart, S., Flagan, R.C., Franchin, A., Guida, R., Hakala, J., Hansel, A., Heinritzi, M., Henschel, H., Jokinen, T., Junninen, H., Kajos, M., Kangasluoma, J., Keskinen, H., Kupc, A., Kurtén, T., Kvashin, A.N., Laaksonen, A., Lehtipalo, K., Leiminger, M., Leppä, J., Loukonen, V., Makhmutov, V., Mathot, S., McGrath, M.J., Nieminen, T., Olenius, T., Onnela, A., Petäjä, T., Riccobono,

F., Riipinen, I., Rissanen, M., Rondo, L., Ruuskanen, T., Santos, F.D., Sarnela, N., Schallhart, S., Schnitzhofer, R., Seinfeld, J.H., Simon, M., Sipilä, M., Stozhkov, Y., Stratmann, F., Tomé, A., Tröstl, J., Tsagkogeorgas, G., Vaattovaara, P., Viisanen, Y., Virtanen, A., Vrtala, A., Wagner, P.E., Weingartner, E., Wex, H., Williamson, C., Wimmer, D., Ye, P., Yli-Juuti, T., Carslaw, K.S., Kulmala, M., Curtius, J., Baltensperger, U., Worsnop, D.R., Vehkamäki, H., Kirkby, J., 2013. Molecular understanding of sulphuric acid–amine particle nucleation in the atmosphere. Nature 502, 359–363. https://doi.org/10.1038/nature12663

Andreae, M.O., 2013. The Aerosol Nucleation Puzzle. Science 339, 911–912. https://doi.org/10.1126/science.1233798

Bachy, A., Aubinet, M., Amelynck, C., Schoon, N., Bodson, B., Delaplace, P., De Ligne, A., Digrado, A., du Jardin, P., Fauconnier, M.-L., Mozaffar, A., Müller, J.-F., Heinesch, B., 2020. Dynamics and mechanisms of volatile organic compound exchanges in a winter wheat field. Atmospheric Environment 221, 117105. https://doi.org/10.1016/j.atmosenv.2019.117105

Bachy, A., Aubinet, M., Amelynck, C., Schoon, N., Bodson, B., Moureaux, C., Delaplace, P., De Ligne, A., Heinesch, B., 2018. Methanol exchange dynamics between a temperate cropland soil and the atmosphere. Atmospheric Environment 176, 229–239. https://doi.org/10.1016/j.atmosenv.2017.12.016

Behera, S.N., Sharma, M., Aneja, V.P., Balasubramanian, R., 2013. Ammonia in the atmosphere: a review on emission sources, atmospheric chemistry and deposition on terrestrial bodies. Environ Sci Pollut Res 20, 8092–8131. https://doi.org/10.1007/s11356-013-2051-9

Berndt, T., Sipilä, M., Stratmann, F., Petäjä, T., Vanhanen, J., Mikkilä, J., Patokoski, J., Taipale, R., Mauldin III, R.L., Kulmala, M., 2014. Enhancement of atmospheric H2SO4 / H2O nucleation: organic oxidation products versus amines. Atmospheric Chemistry and Physics 14, 751–764. https://doi.org/10.5194/acp-14-751-2014

Bianchi, F., Kurtén, T., Riva, M., Mohr, C., Rissanen, M.P., Roldin, P., Berndt, T., Crounse, J.D., Wennberg, P.O., Mentel, T.F., Wildt, J., Junninen, H., Jokinen, T., Kulmala, M., Worsnop, D.R., Thornton, J.A., Donahue, N., Kjaergaard, H.G., Ehn, M., 2019. Highly Oxygenated Organic Molecules (HOM) from Gas-Phase Autoxidation Involving Peroxy Radicals: A Key Contributor to Atmospheric Aerosol. Chem. Rev. 119, 3472–3509. https://doi.org/10.1021/acs.chemrev.8b00395

Bianchi, F., Trostl, J., Junninen, H., Frege, C., Henne, S., Hoyle, C.R., Molteni, U., Herrmann, E., Adamov, A., Bukowiecki, N., Chen, X., Duplissy, J., Gysel, M., Hutterli, M., Kangasluoma, J., Kontkanen, J., Kurten, A., Manninen, H.E., Munch, S., Perakyla, O., Petaja, T., Rondo, L., Williamson, C., Weingartner, E., Curtius, J., Worsnop, D.R., Kulmala, M., Dommen, J., Baltensperger, U., 2016. New particle formation in the free troposphere: A question of chemistry and timing. Science 352, 1109–1112. https://doi.org/10.1126/science.aad5456

Birmili, W., Berresheim, H., 2003. The Hohenpeissenberg aerosol formation experiment (HAFEX): a long-term study including size-resolved aerosol, H2SO4, OH, and monoterpenes measurements. Atmos. Chem. Phys. 16.

Bruns, E.A., Slowik, J.G., El Haddad, I., Kilic, D., Klein, F., Dommen, J., Temime-Roussel, B., Marchand, N., Baltensperger, U., Prévôt, A.S.H., 2017. Characterization of gas-phase organics using proton transfer reaction time-of-flight mass spectrometry: fresh and aged residential wood combustion emissions. Atmos. Chem. Phys. 17, 705–720. https://doi.org/10.5194/acp-17-705-2017

Cai, M., An, C., Guy, C., Lu, C., Mafakheri, F., 2021. Assessing the regional biogenic methanol emission from spring wheat during the growing season: A Canadian case study. Environmental Pollution 287, 117602. https://doi.org/10.1016/j.envpol.2021.117602

Chazeau, B., Temime-Roussel, B., Gille, G., Mesbah, B., D'Anna, B., Wortham, H., Marchand, N., 2021. Measurement report: Fourteen months of real-time characterisation of the submicronic aerosol and its atmospheric dynamics at the Marseille–Longchamp supersite. Atmos. Chem. Phys. 21, 7293–7319. https://doi.org/10.5194/acp-21-7293-2021

Chee, S., Myllys, N., Barsanti, K.C., Wong, B.M., Smith, J.N., 2019. An Experimental and Modeling Study of Nanoparticle Formation and Growth from Dimethylamine and Nitric Acid. J. Phys. Chem. A 123, 5640–5648. https://doi.org/10.1021/acs.jpca.9b03326

Chu, B., Kerminen, V.-M., Bianchi, F., Yan, C., Petäjä, T., Kulmala, M., 2019. Atmospheric new particle formation in China. Atmos. Chem. Phys. 24.

Ciuraru, R., Kammer, J., Decuq, C., Vojkovic, M., Haider, K., Carpentier, Y., Lafouge, F., Berger, C., Bourdat-Deschamps, M., Ortega, I.K., Levavasseur, F., Houot, S., Loubet, B., Petitprez, D., Focsa, C., 2021. New particle formation from agricultural recycling of organic waste products. npj Clim Atmos Sci 4, 1–10. https://doi.org/10.1038/s41612-021-00160-3

Dal Maso, M., Kulmala, M., Riipinen, I., Wagner, R., Hussein, T., Aalto, P.P., Lehtinen, K.E.J., 2005. Formation and growth of fresh atmospheric aerosols: eight years of aerosol size distribution data from SMEAR II, Hyytiälä, Finland. Boreal Environment Research 10, 14.

Dall'Osto, M., Ovadnevaite, J., Ceburnis, D., Martin, D., Healy, R.M., O'Connor, I.P., Kourtchev, I., Sodeau, J.R., Wenger, J.C., O'Dowd, C., 2013a. Characterization of urban aerosol in Cork city (Ireland) using aerosol mass spectrometry. Atmos. Chem. Phys. 13, 4997–5015. https://doi.org/10.5194/acp-13-4997-2013

Dall'Osto, M., Querol, X., Alastuey, A., O'Dowd, C., Harrison, R.M., Wenger, J., Gómez-Moreno, F.J., 2013b. On the spatial distribution and evolution of ultrafine particles in Barcelona. Atmos. Chem. Phys. 13, 741–759. https://doi.org/10.5194/acp-13-741-2013

de Gouw, J., Warneke, C., 2007. Measurements of volatile organic compounds in the earth's atmosphere using proton-transfer-reaction mass spectrometry. Mass Spectrom. Rev. 26, 223–257. https://doi.org/10.1002/mas.20119

Debevec, C., Sauvage, S., Gros, V., Sellegri, K., Sciare, J., Pikridas, M., Stavroulas, I., Leonardis, T., Gaudion, V., Depelchin, L., Fronval, I., Sarda-Esteve, R., Baisnée, D., Bonsang, B., Savvides, C., Vrekoussis, M., Locoge, N., 2018. Driving parameters of biogenic volatile organic compounds and consequences on new particle formation observed at an eastern Mediterranean background site. Atmos. Chem. Phys. 18, 14297–14325. https://doi.org/10.5194/acp-18-14297-2018

Dunn, M.J., Jimenez, J.-L., Baumgardner, D., Castro, T., McMurry, P.H., Smith, J.N., 2004. Measurements of Mexico City nanoparticle size distributions: Observations of new particle formation and growth. Geophysical Research Letters 31, 4. https://doi.org/10.1029/2004GL019483

Duporté, G., Parshintsev, J., Barreira, L.M.F., Hartonen, K., Kulmala, M., Riekkola, M.-L., 2016. Nitrogen-Containing Low Volatile Compounds from Pinonaldehyde-Dimethylamine Reaction in the Atmosphere: A Laboratory and Field Study. Environ. Sci. Technol. 50, 4693–4700. https://doi.org/10.1021/acs.est.6b00270

Feilberg, A., Bildsoe, P., Nyord, T., 2015. Application of PTR-MS for Measuring Odorant Emissions from Soil Application of Manure Slurry. Sensors 15, 1148–1167. https://doi.org/10.3390/s150101148

Fortems-Cheiney, A., Dufour, G., Dufossé, K., Couvidat, F., Gilliot, J.-M., Siour, G., Beekmann, M., Foret, G., Meleux, F., Clarisse, L., Coheur, P.-F., Van Damme, M., Clerbaux, C., Génermont, S., 2020. Do alternative inventories converge on the spatiotemporal representation of spring ammonia emissions in France? Atmos. Chem. Phys. 20, 13481–13495. https://doi.org/10.5194/acp-20-13481-2020

Fuchs, N.A., 1964. The Mechanics of Aerosols. Pergamon Press, Oxford.
Gentner, D.R., Ormeño, E., Fares, S., Ford, T.B., Weber, R., Park, J.-H., Brioude, J., Angevine, W.M., Karlik, J.F., Goldstein, A.H., 2014. Emissions of terpenoids, benzenoids, and other biogenic gas-phase organic compounds from agricultural crops and their potential implications for air quality. Atmospheric Chemistry and Physics 14, 5393–5413. https://doi.org/10.5194/acp-14-5393-2014
Gonzaga Gomez, L., Loubet, B., Lafouge, F., Ciuraru, R., Buysse, P., Durand, B., Gueudet, J.-C., Fanucci, O., Fortineau, A., Zurfluh, O., Decuq, C., Kammer, J., Duprix, P., Bsaibes, S., Truong, F., Gros, V., Boissard, C., 2019. Comparative study of biogenic volatile organic compounds fluxes by wheat, maize and rapeseed with dynamic chambers over a short period in northern France. Atmospheric Environment 214, 116855. https://doi.org/10.1016/j.atmosenv.2019.116855
Gonzaga-Gomez, L., Loubet, B., Lafouge, F., Ciuraru, R., Buysse, P., Durand, B., Gueudet, J.-C., Fanucci, O., Fortineau, A., Zurfluh, O., Decuq, C., Kammer, J., Duprix, P., Bsaibes, S., Truong, F., Gros, V., Boissard, C., 2019. Comparative study of biogenic volatile organic compounds fluxes by wheat, maize and rapeseed with dynamic chambers over a short period in northern France. Atmospheric Environment 116855. https://doi.org/10.1016/j.atmosenv.2019.116855
Graus, M., Eller, A.S.D., Fall, R., Yuan, B., Qian, Y., Westra, P., de Gouw, J., Warneke, C., 2013. Biosphere-atmosphere exchange of volatile organic compounds over C4 biofuel crops. Atmospheric Environment 66, 161–168. https://doi.org/10.1016/j.atmosenv.2011.12.042
Größ, J., Hamed, A., Sonntag, A., Spindler, G., Manninen, H.E., Nieminen, T., Kulmala, M., Hõrrak, U., Plass-Dülmer, C., Wiedensohler, A., Birmili, W., 2018. Atmospheric new particle formation at the research station Melpitz, Germany: connection with gaseous precursors and meteorological parameters. Atmos. Chem. Phys. 18, 1835–1861. https://doi.org/10.5194/acp-18-1835-2018
Haeffelin, M., Barthès, L., Bock, O., Boitel, C., Bony, S., Bouniol, D., Chepfer, H., Chiriaco, M., Cuesta, J., Delanoë, J., Drobinski, P., Dufresne, J.-L., Flamant, C., Grall, M., Hodzic, A., Hourdin, F., Lapouge, F., Lemaître, Y., Mathieu, A., Morille, Y., Naud, C., Noël, V., O'Hirok, W., Pelon, J., Pietras, C., Protat, A., Romand, B., Scialom, G., Vautard, R., 2005. SIRTA, a ground-based atmospheric observatory for cloud and aerosol research. Ann. Geophys. 23, 253–275. https://doi.org/10.5194/angeo-23-253-2005
Hakala, S., Alghamdi, M.A., Paasonen, P., Vakkari, V., Khoder, M.I., Neitola, K., Dada, L., Abdelmaksoud, A.S., Al-Jeelani, H., Shabbaj, I.I., Almehmadi, F.M., Sundström, A.-M., Lihavainen, H., Kerminen, V.-M., Kontkanen, J., Kulmala, M., Hussein, T., Hyvärinen, A.-P., 2019. New particle formation, growth and apparent shrinkage at a rural background site in western Saudi Arabia. Atmos. Chem. Phys. 19, 10537–10555. https://doi.org/10.5194/acp-19-10537-2019
Hakala, S., Vakkari, V., Bianchi, F., Dada, L., Deng, C., Dällenbach, K.R., Fu, Y., Jiang, J., Kangasluoma, J., Kujansuu, J., Liu, Y., Petäjä, T., Wang, L., Yan, C., Kulmala, M., Paasonen, P., 2022. Observed coupling between air mass history, secondary growth of nucleation mode particles and aerosol pollution levels in Beijing. Environ. Sci.: Atmos. 2, 146–164. https://doi.org/10.1039/D1EA00089F
Heintzenberg, J., Wehner, B., Birmili, W., 2007. How to find bananas in the atmospheric aerosol?: new approach for analyzing atmospheric nucleation and growth events. Tellus B 59, 273–282. https://doi.org/10.1111/j.1600-0889.2007.00249.x
Huang, X., Zhou, L., Ding, A., Qi, X., Nie, W., Wang, M., Chi, X., Petäjä, T., Kerminen, V.-M., Roldin, P., Rusanen, A., Kulmala, M., Boy, M., 2016. Comprehensive modelling study on

observed new particle formation at the SORPES station in Nanjing, China. Atmos. Chem. Phys. 16, 2477–2492. https://doi.org/10.5194/acp-16-2477-2016
Hussein, T., Martikainen, J., Junninen, H., Sogacheva, L., Wagner, R., Maso, M.D., Riipinen, I., Aalto, P.P., Kulmala, M., 2008. Observation of regional new particle formation in the urban atmosphere. Tellus B: Chemical and Physical Meteorology 60, 509–521. https://doi.org/10.1111/j.1600-0889.2008.00365.x
Hussein, T., Maso, M.D., Petäjä, T., Koponen, I.K., Paatero, P., Aalto, P.P., Hämeri, K., Kulmala, M., 2005. Evaluation of an automatic algorithm for fitting the particle number size distributions. Boreal Environment Research 10, 20.
IPCC, 2021. Climate Change 2021: The Physical Science Basis. Contribution of Working Group I to the Sixth Assessment Report of the Intergovernmental Panel on Climate Change, Cambridge University Press. ed. Cambridge, UK,.
Irwin, J.S., Binkowski, F.S., 1981. Estimation of the Monin-Obukhov scaling length using on-site instrumentation. Atmospheric Environment (1967) 15, 1091–1094. https://doi.org/10.1016/0004-6981(81)90111-6
Jaatinen, A., Hamed, A., Joutsensaari, J., Mikkonen, S., Birmili, W., Wehner, B., Spindler, G., Wiedensohler, A., Decesari, S., Mircea, M., Facchini, M.C., Junninen, H., Kulmala, M., Lehtinen, K.E.J., Laaksonen, A., 2009. A comparison of new particle formation events in the boundary layer at three different sites in Europe. Boreal Environment Research 14, 19.
Jiang, Z., Grosselin, B., Daële, V., Mellouki, A., Mu, Y., 2017. Seasonal and diurnal variations of BTEX compounds in the semi-urban environment of Orleans, France. Science of The Total Environment 574, 1659–1664. https://doi.org/10.1016/j.scitotenv.2016.08.214
Junninen, H., Hulkkonen, M., Riipinen, I., Nieminen, T., Hirsikko, A., Suni, T., Boy, M., Lee, S.-H., Vana, M., Tammet, H., Kerminen, V.-M., Kulmala, M., 2008. Observations on nocturnal growth of atmospheric clusters. Tellus B: Chemical and Physical Meteorology 60, 365–371. https://doi.org/10.1111/j.1600-0889.2008.00356.x
Kammer, J., Décuq, C., Baisnée, D., Ciuraru, R., Lafouge, F., Buysse, P., Bsaibes, S., Henderson, B., Cristescu, S.M., Benabdallah, R., Chandra, V., Durand, B., Fanucci, O., Petit, J.-E., Truong, F., Bonnaire, N., Sarda-Estève, R., Gros, V., Loubet, B., 2019. Characterization of particulate and gaseous pollutants from a French dairy and sheep farm. Science of The Total Environment 135598. https://doi.org/10.1016/j.scitotenv.2019.135598
Kammer, J., Flaud, P.-M., Chazeaubeny, A., Ciuraru, R., Le Menach, K., Geneste, E., Budzinski, H., Bonnefond, J.M., Lamaud, E., Perraudin, E., Villenave, E., 2020. Biogenic volatile organic compounds (BVOCs) reactivity related to new particle formation (NPF) over the Landes forest. Atmospheric Research 237, 104869. https://doi.org/10.1016/j.atmosres.2020.104869
Kammer, J., Lamaud, E., Bonnefond, J.M., Garrigou, D., Flaud, P.-M., Perraudin, E., Villenave, E., 2018a. Ozone production in a maritime pine forest in water-stressed conditions. Atmospheric Environment. https://doi.org/10.1016/j.atmosenv.2018.10.021
Kammer, J., Perraudin, E., Flaud, P.-M., Lamaud, E., Bonnefond, J.M., Villenave, E., 2018b. Observation of nighttime new particle formation over the French Landes forest. Science of The Total Environment 621, 1084–1092. https://doi.org/10.1016/j.scitotenv.2017.10.118
Kanawade, V.P., Benson, D.R., Lee, S.-H., 2012. Statistical analysis of 4-year observations of aerosol sizes in a semi-rural continental environment. Atmospheric Environment 59, 30–38. https://doi.org/10.1016/j.atmosenv.2012.05.047
Kanawade, V.P., Jobson, B.T., Guenther, A.B., Erupe, M.E., Pressley, S.N., Tripathi, S.N., Lee, S.-H., 2011. Isoprene suppression of new particle formation in a mixed deciduous forest. Atmos. Chem. Phys. 11, 6013–6027. https://doi.org/10.5194/acp-11-6013-2011

Kanawade, V.P., Sebastian, M., Hooda, R.K., Hyvärinen, A.-P., 2022. Atmospheric new particle formation in India: Current understanding and knowledge gaps. Atmospheric Environment 270, 118894. https://doi.org/10.1016/j.atmosenv.2021.118894

Kecorius, S., Zhang, S., Wang, Z., Größ, J., Ma, N., Wu, Z., Ran, L., Hu, M., Wang, P., Ulevičius, V., Wiedensohler, A., 2015. Nocturnal aerosol particle formation in the North China Plain. Lith. J. Phys. 55. https://doi.org/10.3952/physics.v55i1.3057

Kerminen, V.-M., Chen, X., Vakkari, V., Petäjä, T., Kulmala, M., Bianchi, F., 2018. Atmospheric new particle formation and growth: review of field observations. Environ. Res. Lett. 13, 103003. https://doi.org/10.1088/1748-9326/aadf3c

Kesselmeier, Jürgen, Staudt, M., 1999. Biogenic Volatile Organic Compounds (VOC): An Overview on Emission, Physiology and Ecology. Journal of Atmospheric Chemistry 23–88.

Kesselmeier, J, Staudt, M., 1999. Biogenic Volatile Organic Compounds (VOC): An Overview on Emission, Physiology and Ecology 33, 23–88.

Kiendler-Scharr, A., Wildt, J., Maso, M.D., Hohaus, T., Kleist, E., Mentel, T.F., Tillmann, R., Uerlings, R., Schurr, U., Wahner, A., 2009. New particle formation in forests inhibited by isoprene emissions. Nature 461, 381–384. https://doi.org/10.1038/nature08292

Kim, J., Yoon, Y.J., Gim, Y., Choi, J.H., Kang, H.J., Park, K.-T., Park, J., Lee, B.Y., 2019. New particle formation events observed at King Sejong Station, Antarctic Peninsula – Part 1: Physical characteristics and contribution to cloud condensation nuclei. Atmos. Chem. Phys. 19, 7583–7594. https://doi.org/10.5194/acp-19-7583-2019

Kim, Y., Kim, S.-W., Yoon, S.-C., Park, J.-S., Lim, J.-H., Hong, J., Lim, H.-C., Ryu, J., Lee, C.-K., Heo, B.-H., 2016. Characteristics of formation and growth of atmospheric nanoparticles observed at four regional background sites in Korea. Atmospheric Research 12.

Kirkby, J., Duplissy, J., Sengupta, K., Frege, C., Gordon, H., Williamson, C., Heinritzi, M., Simon, M., Yan, C., Almeida, J., Tröstl, J., Nieminen, T., Ortega, I.K., Wagner, R., Adamov, A., Amorim, A., Bernhammer, A.-K., Bianchi, F., Breitenlechner, M., Brilke, S., Chen, X., Craven, J., Dias, A., Ehrhart, S., Flagan, R.C., Franchin, A., Fuchs, C., Guida, R., Hakala, J., Hoyle, C.R., Jokinen, T., Junninen, H., Kangasluoma, J., Kim, J., Krapf, M., Kürten, A., Laaksonen, A., Lehtipalo, K., Makhmutov, V., Mathot, S., Molteni, U., Onnela, A., Peräkylä, O., Piel, F., Petäjä, T., Praplan, A.P., Pringle, K., Rap, A., Richards, N.A.D., Riipinen, I., Rissanen, M.P., Rondo, L., Sarnela, N., Schobesberger, S., Scott, C.E., Seinfeld, J.H., Sipilä, M., Steiner, G., Stozhkov, Y., Stratmann, F., Tomé, A., Virtanen, A., Vogel, A.L., Wagner, A.C., Wagner, P.E., Weingartner, E., Wimmer, D., Winkler, P.M., Ye, P., Zhang, X., Hansel, A., Dommen, J., Donahue, N.M., Worsnop, D.R., Baltensperger, U., Kulmala, M., Carslaw, K.S., Curtius, J., 2016. Ion-induced nucleation of pure biogenic particles. Nature 533, 521–526. https://doi.org/10.1038/nature17953

Kulmala, M., 2003. How Particles Nucleate and Grow. Science 302, 1000–1001.

Kulmala, M., Maso, M.D., Makela, J.M., Pirjola, L., Vakeva, M., Aalto, P., Miikkulainen, P., Hameri, K., O'Dowd, C.D., 2001. On the formation, growth and composition of nucleation mode particles. Tellus B 53, 479–490. https://doi.org/10.1034/j.1600-0889.2001.530411.x

Kulmala, M., Petäjä, T., Ehn, M., Thornton, J., Sipilä, M., Worsnop, D.R., Kerminen, V.-M., 2014. Chemistry of atmospheric nucleation: On the recent advances on precursor characterization and atmospheric cluster composition in connection with atmospheric new particle formation. Annual Review of Physical Chemistry 65, 21–37. https://doi.org/10.1146/annurev-physchem-040412-110014

Kulmala, M., Petäjä, T., Nieminen, T., Sipilä, M., Manninen, H.E., Lehtipalo, K., Dal Maso, M., Aalto, P.P., Junninen, H., Paasonen, P., Riipinen, I., Lehtinen, K.E.J., Laaksonen, A., Kerminen, V.-M., 2012. Measurement of the nucleation of atmospheric aerosol particles. Nat Protoc 7, 1651–1667. https://doi.org/10.1038/nprot.2012.091

Kulmala, M., Vehkamäki, H., Petäjä, T., Dal Maso, M., Lauri, A., Kerminen, V.-M., Birmili, W., McMurry, P.H., 2004. Formation and growth rates of ultrafine atmospheric particles: a review of observations. Journal of Aerosol Science 35, 143–176. https://doi.org/10.1016/j.jaerosci.2003.10.003

Languille, B., Gros, V., Petit, J.-E., Honoré, C., Baudic, A., Perrussel, O., Foret, G., Michoud, V., Truong, F., Bonnaire, N., Sarda-Estève, R., Delmotte, M., Feron, A., Maisonneuve, F., Gaimoz, C., Formenti, P., Kotthaus, S., Haeffelin, M., Favez, O., 2019. Wood burning: A major source of Volatile Organic Compounds during wintertime in the Paris region. Science of The Total Environment 135055. https://doi.org/10.1016/j.scitotenv.2019.135055

Laothawornkitkul, J., Taylor, J.E., Paul, N.D., Hewitt, C.N., 2009. Biogenic volatile organic compounds in the Earth system. New Phytologist 183, 27–51. https://doi.org/10.1111/j.1469-8137.2009.02859.x

Lee, S.-H., Gordon, H., Yu, H., Lehtipalo, K., Haley, R., Li, Y., Zhang, R., 2019. New Particle Formation in the Atmosphere: From Molecular Clusters to Global Climate. J. Geophys. Res. Atmos. 124, 7098–7146. https://doi.org/10.1029/2018JD029356

Lee, S.-H., Young, L.-H., Benson, D.R., Suni, T., Kulmala, M., Junninen, H., Campos, T.L., Rogers, D.C., Jensen, J., 2008. Observations of nighttime new particle formation in the troposphere. J. Geophys. Res. 113, D10210. https://doi.org/10.1029/2007JD009351

Lehtipalo, K., Yan, C., Dada, L., Bianchi, F., Xiao, M., Wagner, R., Stolzenburg, D., Ahonen, L.R., Amorim, A., Baccarini, A., Bauer, P.S., Baumgartner, B., Bergen, A., Bernhammer, A.-K., Breitenlechner, M., Brilke, S., Buchholz, A., Mazon, S.B., Chen, D., Chen, X., Dias, A., Dommen, J., Draper, D.C., Duplissy, J., Ehn, M., Finkenzeller, H., Fischer, L., Frege, C., Fuchs, C., Garmash, O., Gordon, H., Hakala, J., He, X., Heikkinen, L., Heinritzi, M., Helm, J.C., Hofbauer, V., Hoyle, C.R., Jokinen, T., Kangasluoma, J., Kerminen, V.-M., Kim, C., Kirkby, J., Kontkanen, J., Kürten, A., Lawler, M.J., Mai, H., Mathot, S., Mauldin, R.L., Molteni, U., Nichman, L., Nie, W., Nieminen, T., Ojdanic, A., Onnela, A., Passananti, M., Petäjä, T., Piel, F., Pospisilova, V., Quéléver, L.L.J., Rissanen, M.P., Rose, C., Sarnela, N., Schallhart, S., Schuchmann, S., Sengupta, K., Simon, M., Sipilä, M., Tauber, C., Tomé, A., Tröstl, J., Väisänen, O., Vogel, A.L., Volkamer, R., Wagner, A.C., Wang, M., Weitz, L., Wimmer, D., Ye, P., Ylisirniö, A., Zha, Q., Carslaw, K.S., Curtius, J., Donahue, N.M., Flagan, R.C., Hansel, A., Riipinen, I., Virtanen, A., Winkler, P.M., Baltensperger, U., Kulmala, M., Worsnop, D.R., 2018. Multicomponent new particle formation from sulfuric acid, ammonia, and biogenic vapors. Sci. Adv. 4, eaau5363. https://doi.org/10.1126/sciadv.aau5363

Liu, D., Nyord, T., Rong, L., Feilberg, A., 2018. Real-time quantification of emissions of volatile organic compounds from land spreading of pig slurry measured by PTR-MS and wind tunnels. Science of The Total Environment 639, 1079–1087. https://doi.org/10.1016/j.scitotenv.2018.05.149

Loubet, B., Buysse, P., Gonzaga-Gomez, L., Lafouge, F., Ciuraru, R., Decuq, C., Kammer, J., Bsaibes, S., Boissard, C., Durand, B., Gueudet, J.-C., Fanucci, O., Zurfluh, O., Abis, L., Zannoni, N., Truong, F., Baisnée, D., Sarda-Estève, R., Staudt, M., Gros, V., 2021. Volatile organic compound fluxes over a winter wheat field by PTR-Qi-TOF-MS and eddy covariance. Atmospheric Chemistry and Physics Discussions 1–38. https://doi.org/10.5194/acp-2020-1328

Loubet, B., Decuq, C., Personne, E., Massad, R.S., Flechard, C., Fanucci, O., Mascher, N., Gueudet, J.-C., Masson, S., Durand, B., Genermont, S., Fauvel, Y., Cellier, P., 2012. Investigating the stomatal, cuticular and soil ammonia fluxes over a growing tritical crop under high acidic loads. Biogeosciences 9, 1537–1552. https://doi.org/10.5194/bg-9-1537-2012

Loubet, B., Laville, P., Lehuger, S., Larmanou, E., Fléchard, C., Mascher, N., Genermont, S., Roche, R., Ferrara, R.M., Stella, P., Personne, E., Durand, B., Decuq, C., Flura, D., Masson, S., Fanucci, O., Rampon, J.-N., Siemens, J., Kindler, R., Gabrielle, B., Schrumpf, M., Cellier, P., 2011. Carbon, nitrogen and Greenhouse gases budgets over a four years crop rotation in northern France. Plant Soil 343, 109. https://doi.org/10.1007/s11104-011-0751-9

Man, H., Zhu, Y., Ji, F., Yao, X., Lau, N.T., Li, Y., Lee, B.P., Chan, C.K., 2015. Comparison of Daytime and Nighttime New Particle Growth at the HKUST Supersite in Hong Kong. Environ. Sci. Technol. 49, 7170–7178. https://doi.org/10.1021/acs.est.5b02143

McMurry, P.H., Fink, M., Sakurai, H., Stolzenburg, M.R., Mauldin, R.L., Smith, J., Eisele, F., Moore, K., Sjostedt, S., Tanner, D., Huey, L.G., Nowak, J.B., Edgerton, E., Voisin, D., 2005. A criterion for new particle formation in the sulfur-rich Atlanta atmosphere. J. Geophys. Res. 110, D22S02. https://doi.org/10.1029/2005JD005901

Merikanto, J., Spracklen, D.V., Mann, G.W., Pickering, S.J., Carslaw, K.S., 2009. Impact of nucleation on global CCN. Atmos. Chem. Phys. 16.

Nadykto, A.B., Yu, F., 2007. Strong hydrogen bonding between atmospheric nucleation precursors and common organics. Chemical Physics Letters 435, 14–18. https://doi.org/10.1016/j.cplett.2006.12.050

Nemitz, E., Dorsey, J.R., Flynn, M.J., Gallagher, M.W., Hensen, A., Sutton, M.A., 2009. Aerosol fluxes and particle growth above managed grassland 19.

Nilsson, E.D., Rannik, U., Kulmala, M., Buzorius, G., O'Dowd, C.D., 2001. Effects of continental boundary layer evolution, convection, turbulence and entrainment, on aerosol formation. Tellus B 53, 441–461. https://doi.org/10.1034/j.1600-0889.2001.530409.x

Olin, M., Okuljar, M., Rissanen, M.P., Kalliokoski, J., Shen, J., Dada, L., Lampimäki, M., Wu, Y., Lohila, A., Duplissy, J., Sipilä, M., Petäjä, T., Kulmala, M., Dal Maso, M., 2022. Measurement report: Atmospheric new particle formation in a coastal agricultural site explained with binPMF analysis of nitrate CI-APi-TOF spectra. Atmos. Chem. Phys. 22, 8097–8115. https://doi.org/10.5194/acp-22-8097-2022

Ortega, I.K., Suni, T., Boy, M., Grönholm, T., Manninen, H.E., Nieminen, T., Ehn, M., Junninen, H., Hakola, H., Hellén, H., Valmari, T., Arvela, H., Zegelin, S., Hughes, D., Kitchen, M., Cleugh, H., Worsnop, D.R., Kulmala, M., Kerminen, V.-M., 2012. New insights into nocturnal nucleation. Atmos. Chem. Phys. 12, 4297–4312. https://doi.org/10.5194/acp-12-4297-2012

Pang, X., 2015. Biogenic volatile organic compound analyses by PTR-TOF-MS: Calibration, humidity effect and reduced electric field dependency. Journal of Environmental Sciences 32, 196–206. https://doi.org/10.1016/j.jes.2015.01.013

Parker, D.B., Gilley, J., Woodbury, B., Kim, K.-H., Galvin, G., Bartelt-Hunt, S.L., Li, X., Snow, D.D., 2013. Odorous VOC emission following land application of swine manure slurry. Atmospheric Environment 66, 91–100. https://doi.org/10.1016/j.atmosenv.2012.01.001

Paulot, F., Crounse, J.D., Kjaergaard, H.G., Kroll, J.H., Seinfeld, J.H., Wennberg, P.O., 2009. Isoprene photooxidation: new insights into the production of acids and organic nitrates. Atmos. Chem. Phys. 9, 1479–1501. https://doi.org/10.5194/acp-9-1479-2009

Potard, K., Monard, C., Le Garrec, J.-L., Caudal, J.-P., Le Bris, N., Binet, F., 2017. Organic amendment practices as possible drivers of biogenic Volatile Organic Compounds emitted

by soils in agrosystems. Agriculture, Ecosystems & Environment 250, 25–36. https://doi.org/10.1016/j.agee.2017.09.007
Potier, E., Ogée, J., Jouanguy, J., Lamaud, E., Stella, P., Personne, E., Durand, B., Mascher, N., Loubet, B., 2015. Multilayer modelling of ozone fluxes on winter wheat reveals large deposition on wet senescing leaves. Agricultural and Forest Meteorology 211–212, 58–71. https://doi.org/10.1016/j.agrformet.2015.05.006
Rose, C., Sellegri, K., Asmi, E., Hervo, M., Freney, E., Junninen, H., Duplissy, J., Sipilä, M., Kontkanen, J., Lehtipalo, K., Kulmala, M., 2014. Major contribution of neutral clusters to new particle formation in the free troposphere. Atmospheric Chemistry and Physics Discussions 14, 18355–18388. https://doi.org/10.5194/acpd-14-18355-2014
Rose, C., Zha, Q., Dada, L., Yan, C., Lehtipalo, K., Junninen, H., Mazon, S.B., Jokinen, T., Sarnela, N., Sipilä, M., Petäjä, T., Kerminen, V.-M., Bianchi, F., Kulmala, M., 2018. Observations of biogenic ion-induced cluster formation in the atmosphere. Sci. Adv. 4, eaar5218. https://doi.org/10.1126/sciadv.aar5218
Salimi, F., Rahman, Md.M., Clifford, S., Ristovski, Z., Morawska, L., 2017. Nocturnal new particle formation events in urban environments. Atmos. Chem. Phys. 17, 521–530. https://doi.org/10.5194/acp-17-521-2017
Salma, I., Borsos, T., Weidinger, T., Aalto, P., Hussein, T., Maso, M.D., Kulmala, M., 2011. Production, growth and properties of ultrafine atmospheric aerosol particles in an urban environment. Atmos. Chem. Phys. 15.
Schobesberger, S., Praplan, A., Junninen, H., Bianchi, F., Lönn, G., Ehn, M., Lehtipalo, K., Dommen, J., Ehrhart, S., Franchin, A., Ortega, I.K., Riccobono, F., Duplissy, J., Rissanen, M., Sipilä, M., Petäjä, T., Kulmala, M., Donahue, N.M., Worsnop, D.R., CLOUD Collaboration, 2013. Measuring composition and growth of ion clusters of sulfuric acid, ammonia, amines and oxidized organics as first steps of nucleation in the CLOUD experiment. Presented at the NUCLEATION AND ATMOSPHERIC AEROSOLS: 19th International Conference, Fort Collins, Colorado, USA, pp. 298–301. https://doi.org/10.1063/1.4803262
Seinfeld, J., Pandis, S.N., 2006. Atmospheric Chemistry and Physics: From Air Pollution to Climate Change, 3rd Edition | Wiley. Wilwy.
Stanier, C.O., Khlystov, A.Y., Pandis, S.N., 2004. Nucleation Events During the Pittsburgh Air Quality Study: Description and Relation to Key Meteorological, Gas Phase, and Aerosol Parameters Special Issue of *Aerosol Science and Technology* on Findings from the Fine Particulate Matter Supersites Program. Aerosol Science and Technology 38, 253–264. https://doi.org/10.1080/02786820390229570
Stella, P., Personne, E., Lamaud, E., Loubet, B., Trebs, I., Cellier, P., 2013. Assessment of the total, stomatal, cuticular, and soil 2 year ozone budgets of an agricultural field with winter wheat and maize crops: STOMATAL AND NONSTOMATAL OZONE BUDGETS. Journal of Geophysical Research: Biogeosciences 118, 1120–1132. https://doi.org/10.1002/jgrg.20094
Suni, T., Kulmala, M., Hirsikko, A., Bergman, T., Laakso, L., Aalto, P.P., Leuning, R., Cleugh, H., Zegelin, S., Hughes, D., van Gorsel, E., Kitchen, M., Vana, M., Horrak, U., Mirme, S., Mirme, A., Sevanto, S., Twining, J., Tadros, C., 2008. Formation and characteristics of ions and charged aerosol particles in a native Australian Eucalypt forest. Atmos. Chem. Phys. 11.
Svenningsson, B., Arneth, A., Hayward, S., Holst, T., Massling, A., Swietlicki, E., Hirsikko, A., Junninen, H., Riipinen, I., Vana, M., Maso, M.D., Hussein, T., Kulmala, M., 2008. Aerosol particle formation events and analysis of high growth rates observed above a subarctic wetland–forest mosaic. Tellus B: Chemical and Physical Meteorology 60, 353–364. https://doi.org/10.1111/j.1600-0889.2008.00351.x

Tani, A., Hayward, S., Hewitt, C.N., 2003. Measurement of monoterpenes and related compounds by proton transfer reaction-mass spectrometry (PTR-MS). International Journal of Mass Spectrometry 223–224, 561–578. https://doi.org/10.1016/S1387-3806(02)00880-1

Vehkamaki, H., Maso, M.D., Hussein, T., Flanagan, R., Hyvarinen, A., Lauros, J., Merikanto, J., Monkkonen, P., Pihlatie, M., Salminen, K., Sogacheva, L., Thum, T., Ruuskanen, T.M., Keronen, P., Aalto, P.P., Hari, P., Lehtinen, K.E.J., Rannik, U., Kulmala, M., 2004. Atmospheric particle formation events at Va¨rrio¨ measurement station in Finnish Lapland 1998–2002. Atmos. Chem. Phys. 9.

Wang, Z., Wu, Z., Yue, D., Shang, D., Guo, S., Sun, J., Ding, A., Wang, L., Jiang, J., Guo, H., Gao, J., Cheung, H.C., Morawska, L., Keywood, M., Hu, M., 2017. New particle formation in China: Current knowledge and further directions. Science of The Total Environment 577, 258–266. https://doi.org/10.1016/j.scitotenv.2016.10.177

Wehner, B., Siebert, H., Stratmann, F., Tuch, T., Wiedensohler, A., PetäJä, T., Dal Maso, M., Kulmala, M., 2007. Horizontal homogeneity and vertical extent of new particle formation events. Tellus B: Chemical and Physical Meteorology 59, 362–371. https://doi.org/10.1111/j.1600-0889.2007.00260.x

Wonaschütz, A., Demattio, A., Wagner, R., Burkart, J., Zíková, N., Vodička, P., Ludwig, W., Steiner, G., Schwarz, J., Hitzenberger, R., 2015. Seasonality of new particle formation in Vienna, Austria – Influence of air mass origin and aerosol chemical composition. Atmospheric Environment 118, 118–126. https://doi.org/10.1016/j.atmosenv.2015.07.035

Woodbury, B.L., Gilley, J.E., Parker, D.B., Marx, D.B., Miller, D.N., Eigenberg, R.A., 2014. Emission of Volatile Organic Compounds after Land Application of Cattle Manure. J. Environ. Qual. 43, 1207–1218. https://doi.org/10.2134/jeq2013.05.0185

Wu, Z., Hu, M., Liu, S., Wehner, B., Bauer, S., Ma ßling, A., Wiedensohler, A., Petäjä, T., Dal Maso, M., Kulmala, M., 2007. New particle formation in Beijing, China: Statistical analysis of a 1-year data set. J. Geophys. Res. 112, D09209. https://doi.org/10.1029/2006JD007406

Xiao, M., Hoyle, C.R., Dada, L., Stolzenburg, D., Kürten, A., Wang, M., Lamkaddam, H., Garmash, O., Mentler, B., Molteni, U., Baccarini, A., Simon, M., He, X.-C., Lehtipalo, K., Ahonen, L.R., Baalbaki, R., Bauer, P.S., Beck, L., Bell, D., Bianchi, F., Brilke, S., Chen, D., Chiu, R., Dias, A., Duplissy, J., Finkenzeller, H., Gordon, H., Hofbauer, V., Kim, C., Koenig, T.K., Lampilahti, J., Lee, C.P., Li, Z., Mai, H., Makhmutov, V., Manninen, H.E., Marten, R., Mathot, S., Mauldin, R.L., Nie, W., Onnela, A., Partoll, E., Petäjä, T., Pfeifer, J., Pospisilova, V., Quéléver, L.L.J., Rissanen, M., Schobesberger, S., Schuchmann, S., Stozhkov, Y., Tauber, C., Tham, Y.J., Tomé, A., Vazquez-Pufleau, M., Wagner, A.C., Wagner, R., Wang, Y., Weitz, L., Wimmer, D., Wu, Y., Yan, C., Ye, P., Ye, Q., Zha, Q., Zhou, X., Amorim, A., Carslaw, K., Curtius, J., Hansel, A., Volkamer, R., Winkler, P.M., Flagan, R.C., Kulmala, M., Worsnop, D.R., Kirkby, J., Donahue, N.M., Baltensperger, U., El Haddad, I., Dommen, J., 2021. The driving factors of new particle formation and growth in the polluted boundary layer. Atmospheric Chemistry and Physics 21, 14275–14291. https://doi.org/10.5194/acp-21-14275-2021

Xiao, S., Wang, M.Y., Yao, L., Kulmala, M., Zhou, B., Yang, X., Chen, J.M., Wang, D.F., Fu, Q.Y., Worsnop, D.R., Wang, L., 2015. Strong atmospheric new particle formation in winter in urban Shanghai, China. Atmos. Chem. Phys. 15, 1769–1781. https://doi.org/10.5194/acp-15-1769-2015

Xu, C.-X., Jiang, S., Liu, Y.-R., Feng, Y.-J., Wang, Z.-H., Huang, T., Zhao, Y., Li, J., Huang, W., 2020. Formation of atmospheric molecular clusters of methanesulfonic acid–Diethylamine complex and its atmospheric significance. Atmospheric Environment 226, 117404. https://doi.org/10.1016/j.atmosenv.2020.117404

Yao, L., Garmash, O., Bianchi, F., Zheng, J., Yan, C., Kontkanen, J., Junninen, H., Mazon, S.B., Ehn, M., Paasonen, P., Sipilä, M., Wang, M., Wang, X., Xiao, S., Chen, H., Lu, Y., Zhang, B., Wang, D., Fu, Q., Geng, F., Li, L., Wang, H., Qiao, L., Yang, X., Chen, J., Kerminen, V.-M., Petäjä, T., Worsnop, D.R., Kulmala, M., Wang, L., 2018. Atmospheric new particle formation from sulfuric acid and amines in a Chinese megacity 5.

Young, L.-H., Lee, S.-H., Kanawade, V.P., Hsiao, T.-C., Lee, Y.L., Hwang, B.-F., Liou, Y.-J., Hsu, H.-T., Tsai, P.-J., 2013. New particle growth and shrinkage observed in subtropical environments. Atmospheric Chemistry and Physics 13, 547–564. https://doi.org/10.5194/acp-13-547-2013

Yu, F., Luo, G., Nair, A.A., Schwab, J.J., Sherman, J.P., Zhang, Y., 2020. Wintertime new particle formation and its contribution to cloud condensation nuclei in the Northeastern United States. Atmospheric Chemistry and Physics 20, 2591–2601. https://doi.org/10.5194/acp-20-2591-2020

Yu, H., Ren, L., Kanawade, V.P., 2017. New Particle Formation and Growth Mechanisms in Highly Polluted Environments. Curr Pollution Rep 3, 245–253. https://doi.org/10.1007/s40726-017-0067-3

Zhu, B., Wang, H., Shen, L., Kang, H., Yu, X., 2013. Aerosol spectra and new particle formation observed in various seasons in Nanjing. Adv. Atmos. Sci. 30, 1632–1644. https://doi.org/10.1007/s00376-013-2202-4

Zhu, Y.-P., Liu, Y.-R., Huang, T., Jiang, S., Xu, K.-M., Wen, H., Zhang, W.-J., Huang, W., 2014. Theoretical Study of the Hydration of Atmospheric Nucleation Precursors with Acetic Acid. J. Phys. Chem. A 118, 7959–7974. https://doi.org/10.1021/jp506226z